ADVANCED ENERGY & SUSTAINABILITY RESEARCH
Open Access
www.advenergysustres.com

Electronic View of Triboelectric Nanogenerator for Energy Harvesting: Mechanisms and Applications

Qiuyang Lu, Mingzi Sun, Bolong Huang, and Zhong Lin Wang**

Harvesting energy from rain, waves, and river flows has been an old problem for over 100 years. Hydropower is capable of the features of huge quantity, low cost, and renewability. To date, the investigations on triboelectrification have shed a light on flexible and sufficient energy harvesting methods from hydropower or ambient motions. A triboelectric nanogenerator (TENG) has become the most promising energy harvesting system in recent years. Herein, the background of hydropower is first introduced to highlight the urgent need of novel energy conversion devices. Meanwhile, the detailed working principle of contact electrification (CE) is summarized by focusing on the origins of charge and how such a charge is induced. With systematic studies, the common modes of charge generation systems are well investigated. Then, the fabrications of various types of CE-based devices are introduced with the potential modifications to achieve high applicability in specific circumstances. In addition, the multifunctional devices for distinctive energy harvesting processes constructed by TENG are also reviewed. Due to real-time response to environmental variation, TENG-based self-powered sensors and wearable healthcare devices have also become promising candidates in the scientific field as well as different aspects of daily life.

1. Introduction

The world is facing an ongoing energy crisis, which is caused by constantly declined fossil fuel capacity and induced environmental pollutions in both atmosphere and ocean. Despite the construction of solar panels for harvesting solar and wind energy, the overall production still dissatisfies the requirements for loading enormous rising technologies and diverse devices. Although enormous research has been dedicated to investigate novel energy harvesting strategies, most of the inventions cost astonishingly high prices or require complicated equipment to achieve utilizable output, which blocks further practical developments. Hydropower is a renewable, sustainable energy source contained in moving water and continuously renewed by the sun. Owing to the huge quantity, low cost, and broad applications, hydropower becomes a superior and desirable candidate for the manufacture of portable energy supplies. To date, the typical method of harvesting kinetic energy contained in water movements is well known as the electromagnetic generator (EMG). However, such a strategy usually requires the relatively high speed of the water movement, which induces significant obstacles to further development.

Nanogenerator was invented for converting nanoscale mechanical energy into electrical energy via electrical polarization,[1] which was unprecedentedly proposed by Wang and co-workers.[2] When bending a piezoelectric zinc oxide nanowire, charges on the surface moved and rearranged, creating a strain field. Nowadays, the studies of flexible nanogenerators have been extensively and comprehensively advanced. These works indicate that the integration of flexibility and stretchability of the nanogenerator device is the predominant factor determining the performances and durability of practical applications, such as low-power portable electronics and self-powered sensors.[3] This new concept of nanogenerator relying on piezoelectrification and triboelectrification can constantly harvest mechanical energy contained in an ambient environment, thereby constituting a new type of self-powered sustainable energy supply. A large amount of nanogenerators has so far been specifically designed and fabricated on account of complex circumstances and triggers. The piezoelectric nanogenerator is typically applied in the system with asymmetric pressures; the strain can introduce the electrical polarization and charge

Q. Lu, M. Sun, Prof. B. Huang
Department of Applied Biology and Chemical Technology
The Hong Kong Polytechnic University
Hung Hom, Kowloon, Hong Kong SAR, China
E-mail: bhuang@polyu.edu.hk

Prof. Z. L. Wang
Beijing Institute of Nanoenergy and Nanosystems
Chinese Academy of Sciences
Beijing 100083, China
E-mail: zlwang@gatech.edu

Prof. Z. L. Wang
School of Materials Science and Engineering
Georgia Institute of Technology
Atlanta, GA 30332, USA

The ORCID identification number(s) for the author(s) of this article can be found under https://doi.org/10.1002/aesr.202000087.

DOI: 10.1002/aesr.202000087

redistribution on the wire surface, and the commingled effects create a charge flow.[4] As for the triboelectric nanogenerator (TENG), the working principle is predicated on the contact electrification (CE) effect. The area power density of a single nanogenerator device[5] can reach 500 Wm^{-2}, and the volume power density can reach 15 MWm^{-3}. The synchronous energy conversion efficiency of ≈70% has also been demonstrated.[6]

Considering the unavoidable demerits in current hydropower-harvest EMG systems, the high-performance flexible TENGs have great potentials for improving the conversion rate and broadening the applicable range. TENG can directly convert diverse types of mechanical energy into electricity, such as rainfall, water flow, and other kinds of water motions commonly emerging in our daily life. The different working mechanisms in EMG and TENG lead to extensive differences in the output performances. EMGs can be driven by the relative motions between a conductor and a magnet, whereas TENGs generate a displacement current originated from the triboelectric potential difference between two sections of a device. The fundamental function process of TENG devices preliminarily starts with the contact induced by an external force; then, the electrons distributed inside of materials and on the surface would change, because the contacted state alters the potentials of both objects. After separating, electrons remain in the rearranged positions for a while, causing a triboelectrification phenomenon and producing electrical signals in the external circuit. The first comprehensive study about TENG and its working principle is reported by Wang and co-workers in 2012.[7] They claimed the power density, and the total efficiency of devices with different structures can reach 50 $mW\,cm^2$ and 50%,[5,8] respectively. For further advancing and constituting high-efficient, low-cost, and biocompatible practical TENG devices, massive strides have been made for improving the functional properties by rational design and structural modification.

The composition of a certain TENG device can be complicated but unlimited, in which the materials are normally metal and dielectric because of their excellent characteristics in electron transmission and flexibility. Large amounts of works have identified that the material choice of TENG is abundant. In particular, TENG devices are superior energy harvesters for hydropower converting when utilized in the solid–water interface, because the cycling motion of raindrops or waves can induce regular contact-separation dynamics. However, TENGs possess great advantages for their much fewer obstacles in the prerequisite energy qualities. In comparison, the traditional EMGs-based water motion converters often require a high relative motion rate for achieving a qualified output efficiency while TENG can even harvest energy from a slow movement. Therefore, this review aims to present an adequate summary of recent investigations and designs about the TENG devices and their distinctive working mechanisms. The applications and affecting parameters of each mode are also addressed. As a promising strategy of energy generation and revolution in novel energetic systems, TENGs are capable of harvesting diverse types of kinetic energies and superior in practical applications to a wider range.

2. Working Principle

CE is the scientific term for triboelectric,[9] which means electricity can be produced by physical contact. Notably, the mechanical friction is not necessary even though generally mentioned in most static electricity cases. Although CE exists commonly in our daily life, the origin of CE keeps undisposed for a long period. In recent years, researchers paid attention to this kind of unexploited energy and started to retrofit it into efficient energy sources. For this purpose, the accurate function progress and underlying mechanisms need to be explained and demonstrated. According to experimental investigations, the occurrence of CE fails to be attributed to the ion transfer. **Figure 1**a shows the experimental data about the residual charges on the Ti–Al_2O_3 TENG surface under different temperatures.[10] As shown in the graph, the residual charge percentage continuously decreases along with the increase in temperature. If ion transfer is assumed to be the reason for potential variation in triboelectrification, more triboelectric electrons should be transferred at a higher temperature, because this follows the Boltzmann distribution. Consequently, ion transfer has been ruled out due to the unmatched experimental results.

Then, the electron transfer has been accommodated to explain the origin of CE. Even if electron transfer has been proved to be the origin of the CE phenomenon in the solid–solid model, the rational explanation of triboelectrification in water–solid cases remains controversial. The fluidity and dispersibility are the typical features of liquid, which cause diffused ions and electrons, and the absorption phenomenon after contact brings more uncertainty for identifying the origin of triboelectrification. For better assessing this problem, a series of experiments investigating contact-separation states between polytetrafluoroethylene (PTFE) film and distinct liquids have been implemented.[11] First, deionized (DI) water was utilized as the liquid dielectric, and PTFE membrane was deposited on the fluorine-doped tin oxide (FTO) glass as the conductor. The experiment process is shown in Figure 1b as a squeezing method, and the object is only one drop of water. The results indicated that the produced charge density was in the scale of 1 $nC\,cm^{-2}$ when the volume of liquids is 50 μL, which is ten times higher than the theoretical calculation results based on the ion transfer model, which means that the charges accumulated on the surface are dominated by electron transfer.

In the experiment design, the researchers assumed that the charge aggregating was purely generated by ion transfer between the water droplet and the glass in the theoretical analysis. They calculated the ideal situation when all the OH^- was absorbed onto the PTFE surface; however, it still dissatisfied the quantity of detected charges in experiments. These results indicated that electron transfer must be considered for the excess part of charges. CE is a complex process even with up-to-date technologies. However, with the invention of Kelvin probe force microscopy (KPFM), researchers started to establish a nanoscale understanding of the contact process. KPFM is a surface potential microscopy that is capable of observing the surface features at atomic scales.[9] A systematic review of the mechanism of CE using KPFM has been proposed by Wang and co-workers, and the dominant mechanism of CE proposed by electron cloud overlapping was revealed as well (Figure 1c).[10] This work pinpoints the general explanations for all CEs created by conventional materials. It is worth mentioning that polymers and noncrystalline materials are not conformed to the band structure theory, and a general and applicable model is necessary for the CE.

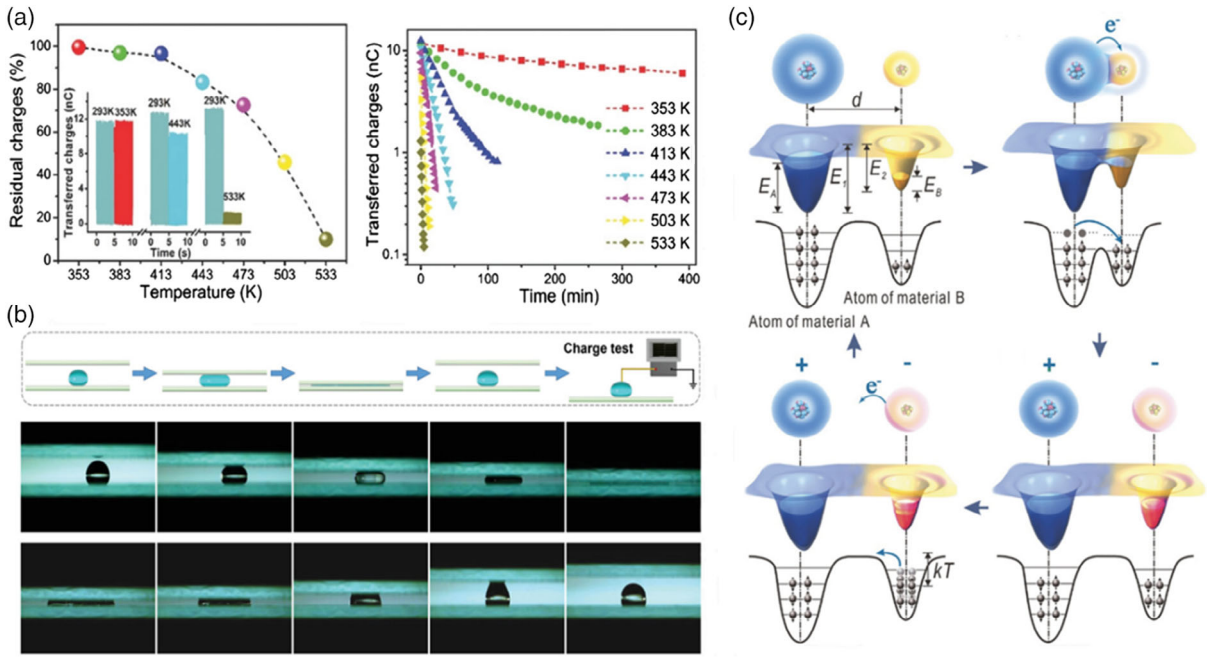

Figure 1. a) The percentage and transferred charges of residual charges of the TENG at different temperatures. Reproduced with permission.[10] Copyright 2018, Wiley VCH. b) Schematic illustration and real photographs of testing the charge on a water droplet after periodic squeezing. Reproduced with permission.[11] Copyright 2020, Wiley VCH. c) An electron-cloud model for explaining CE and charge transfer mechanism. Reproduced with permission.[10] Copyright 2018, Wiley VCH.

To clarify, electrons occupying specific atomic or molecular orbitals are both assumed as an electron cloud model. Before contact, the electrons are bound inside of the object due to the respective potential wells. When an external force is applied to the two objects, the two individual potential wells overlap with each other and become an asymmetric double-well potential.[10,12] Then, the electrons can easily migrate from the higher energy level to the lower side in the double well. Due to the strong overlapping, the obstacles and binding forces to the electrons are hindered, and the interactions between molecules and electrons are also reconstructed. As a result, the electrons of one atom can be transferred to another, leading to the CE phenomenon. After separating, most of the electrons are reserved in the new locations, and the potential of each object changes. Such a variation exhibits an electrical single, which is directly detectable when loading an external measurement between the two objects. Applying a KPFM analysis with a Pt atomic force microscope (AFM) tip on the SiO_2 surface in tapping mode,[13] the nanoscale observation of electron stacking on the surface is implemented. The tip continuously scans over an area of 5 μm in dimension, and the surface charge density of this certain position on the SiO_2 arises, and then gets to saturation after the eighth cycle. In the solid–water interface, the triboelectrification effect can also make water and contact interface charged with similar principles. The contact-separation motion between the water and the insulative layer of a TENG device produces electrons redistribution. In each circle, the insulator unit prevents electron leakage and induces an unbalanced potential between electrodes. If an external circuit is connected, the current and voltage can be detected. This is the work progresses of fundamental contact-separation water–solid TENG.

3. Operation Modes

3.1. CE in Metal–Solid Cases

The CE phenomenon (**Figure 2**a) is generally observed in nature, and with the advent of TENG devices, it would become an alternative to harvest ambient energy as portable energy sources.[14] The origin of it is consistently studied by multiple methods. The Pt tip and SiO_2 surface are introduced as a metal–solid model in the previous section (Figure 2b).[15] The AFM tip has two function modes, which induce reverse results when scanning on similar surfaces, respectively,[16] thus utilized for detecting how the contact motions interfere with charge transfer on the interface. First, the Pt AFM tip was working in a taping mode, and a constant force drove the tip scanning on the SiO_2 surface with a regular motion. Charge transfer was triggered on the interface. According to the assessed results, electrons took a relatively long time to efficiently stack on the surface and reach the saturation point (Figure 2c).[16b] When changed to the sliding mode, the probe continuously slipped on the substrate, and the charges were transferred at a higher rate, made it a more efficient mode.

This study aimed to investigate if the sliding motion in triboelectrification behavior creates a more sufficient charge transfer effect compared with the taping mode (Figure 2d).[16a] When examined under the equivalent conditions, the sliding mode triboelectrification enables high charge transfer efficiency than the taping mode. However, the consumed time of each mode varied due to the difference in charge transfer speed. The surface charge density saturation limit keeps constant, because it

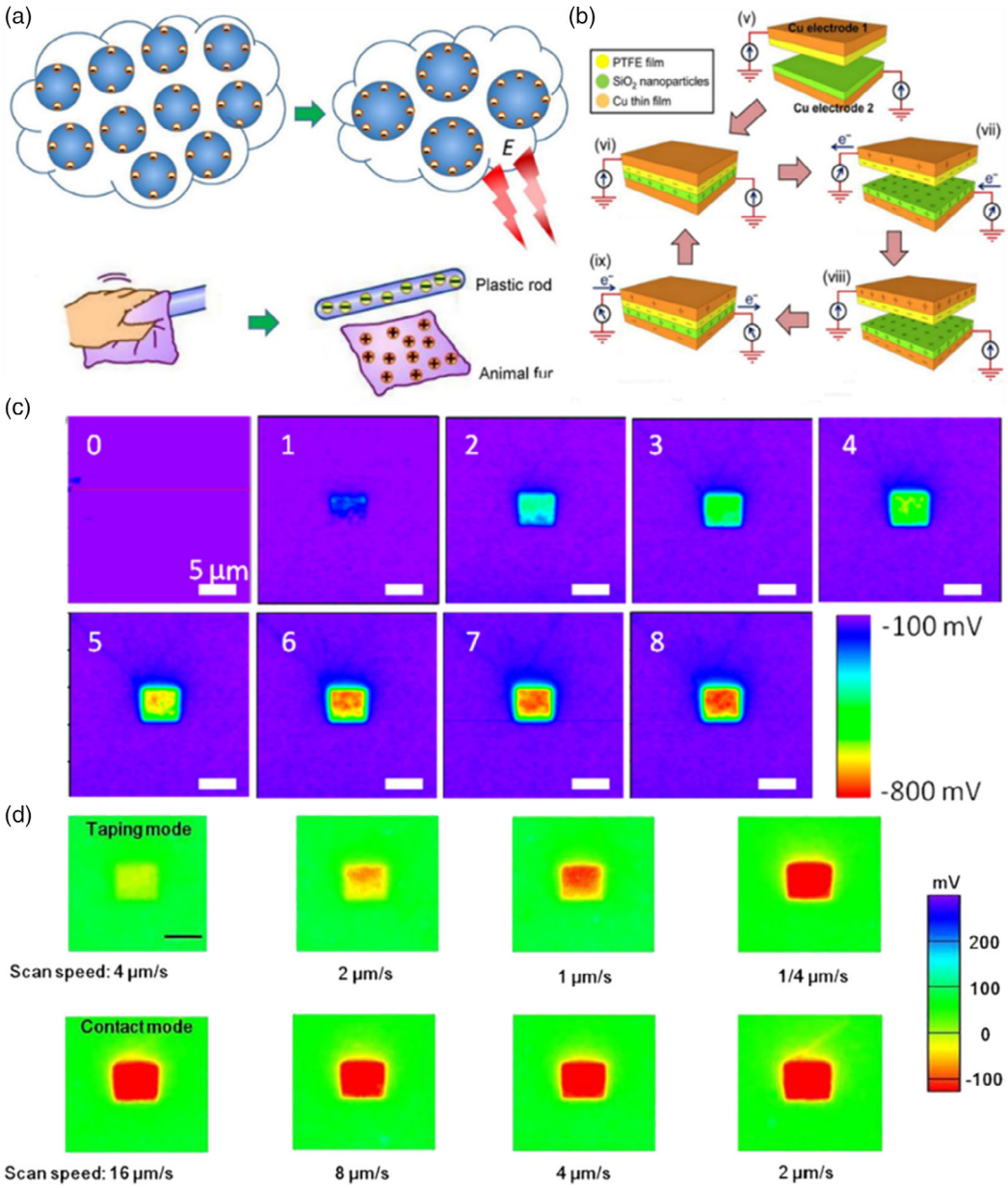

Figure 2. a) Representative contact electric phenomenon in daily life. Reproduced with permission.[14b] Copyright 2019, Elsevier. b) Schematic illustration of CE. Reproduced with permission.[15] Copyright 2014, American Chemical Society. c) Triboelectric charge accumulation from an initial state to the final state after the eighth rubbing cycle. Reproduced with permission.[16b] Copyright 2013, American Chemical Society. d) Surface potential mapping by AFM probe in the tapping mode and the contact mode. Reproduced with permission.[16a] Copyright 2016, Springer.

depends on the breakdown threshold of the specific surface in the air.[13] The saturation limit and the sign of the charge transferred onto a dielectric surface can be altered by varying the relative potential distinction.[17] By controlling the bias on the tip from −5to +5 V, the charges on the surface also vary from negative to positive, indicating a change of the insulator surface from the electron adaptor to a "reservoir." However, the experiment suggested that no charge transmission occurred when the bias was 3–4 V. It introduced an additional pathway for further understanding of the mechanism of CE. The metal is typically characterized by its Fermi level when electrons with higher energy above the Fermi level are normally easy for depletion. Depending on the semiconductor theory, the dielectric material is assumed to have the conduction band and valence band, and between them, there are various defects states and surface states. Under the metal's Fermi level, orbitals are primarily occupied with electrons in the ground state. When the edge of the valence band of the dielectric is under the Fermi level of the metal during the contact, electrons occasionally escape from the metal. The electrons often populated low energy states compared with the Fermi level of metal, resulting in the negative charges assembled on the dielectric surface. If a negative bias is applied on the tip,

which induces an energy shift of the valence band to be even lower corresponding to the initial state, more electrons would be depleted. If a positive bias is applied, the energy of the valence band tends to shift to a higher level depending on the bias magnitude. If the introduced energy state is similar to the Fermi level, there should be no electron exchange. The electrons also have a chance to be transferred to the metal if the electrons in dielectric materials occupied a higher energy level than the Fermi level.

3.2. CE in Liquid–Solid Cases

CE not only occurs on the solid–solid interface but also in the water–solid pairs. The raindrop falling and thunder both originate from the charge transfer and the electron gathering in water–water or water–gas systems. The contact-separation concerning charge transfer in the water–water or water–gas model is similar to the solid–solid model. By applying a load in the external circuit, the produced current can be directly detected between electrodes. If the aqueous dielectric material rolls off from the conductor, the triboelectric potential of each object is unbalanced because of the residual electrons, and a reverse current flow is produced. This leads to an alternating current (AC) characteristic of triboelectrification driven by the cycling motion triggering.

3.2.1. Contact-Separation Mode

The demonstration of contact-separation mode is shown in **Figure 3**a by Liang et al.[18] In most of the cases, the device was constituted by polydimethylsiloxane (PDMS), and water was used as the contact object (Figure 3b).[19] Back in 2013, the contact-separation mode TENG was reported by Lin et al., which insightfully investigated the advantages of the TENG device in harvesting the intermittent irregular vibration energy from the ambient environment[20] (Figure 3c). The copper film was utilized as both the substrate of water and the electrode on one side, and the other electrode was adherent on the back of the PDMS film, which formed an external circuit for detection and observation. When water flowed on the PDMS surface, the water surface was positively charged and conversely left the PDMS with

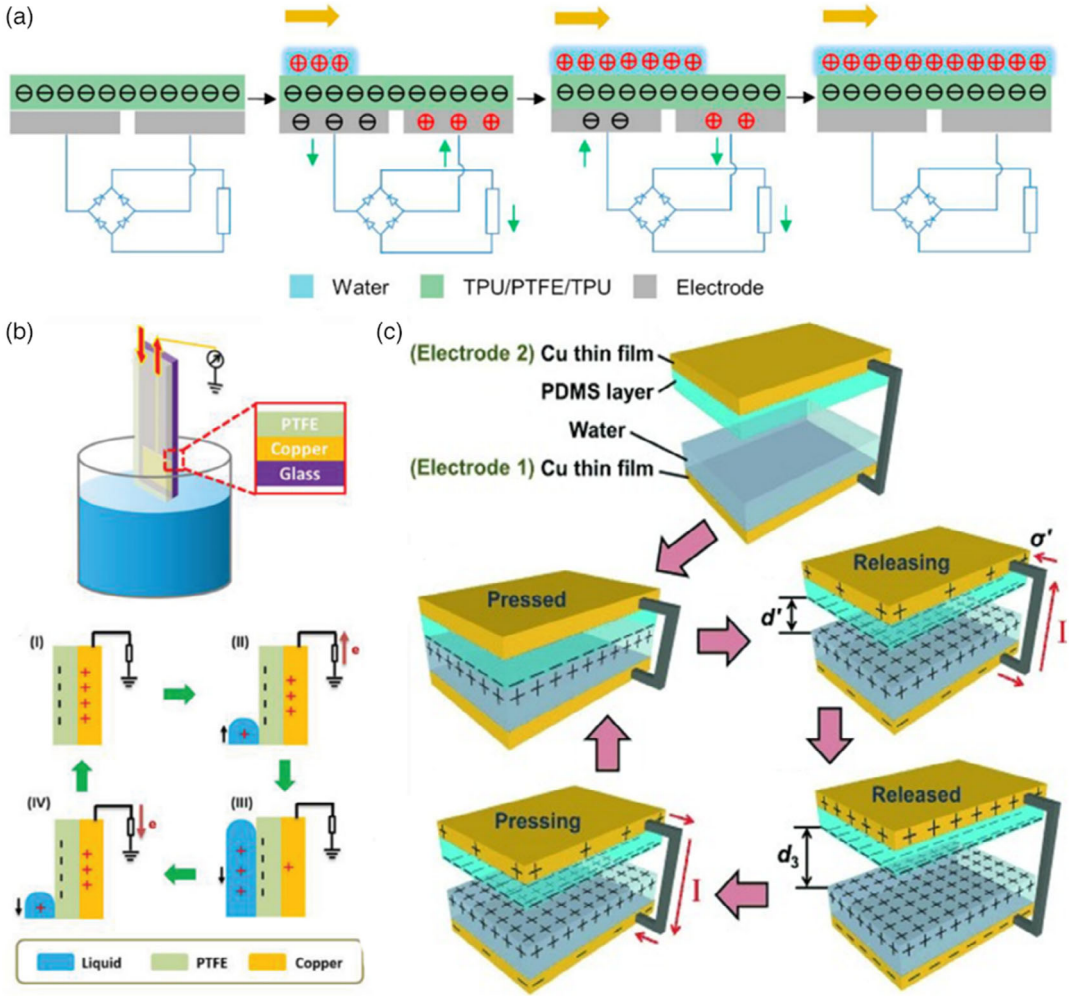

Figure 3. Schematic illustration of the CE modes. a) The CE mechanism of the water–solid TENG. Reproduced with permission.[18] Copyright 2019, Elsevier. b) A simple contact-separation TENG operates with submerged into the water container. Reproduced with permission.[19] Copyright 2019, Wiley VCH. c) A two-electrode based contact-separation TENG. Reproduced with permission.[20] Copyright 2013, Wiley VCH.

negative charges. The sign of charges on two sides is determined by the ionization phenomenon of the surface group. Current flow was generated from the electrode on the PDMS film to that connected to the water while the two objects were separated. Hence, an alternative current was generated via the continuous contact-separation motions. It has been proved that DI water can produce the highest charge transfer efficiency with a charge density of 31.3 μC m^{-2}. The experiment also assessed the output performances with the tap water and the NaCl solution (0.6 M),[21] displaying the performances of 15.02 and 5.7 μC m^{-2}, respectively. The reduced output indicates that the ions in the liquid compensate for the triboelectric charges in the interface, and the electrostatic-induced charges in the back electrons also decrease.

3.2.2. Single-Electrode Mode

Single-electrode mode is a commonly used method for TENG application in harvesting hydropower. In previous sections, researchers have demonstrated the necessity of relative position changes by an external triggering or other cycling motion in TENG. However, the single-electrode mode facilitates spontaneous energy generation with a stationary state, because the movements are provided by the natural falling or rolling motions of water droplets. The working principle of a single-electrode mode TENG nanogenerator is exhibited in **Figure 4**.[22]

The device is normally constituted with a hydrophobic layer such as PTFE[19] with a copper electrode in the back connected to another electrode or the ground. A stacked layer of poly(methyl methacrylate) (PMMA) subtract is also used for a dielectric plane. The electrode is connected to an ammeter for the charge flow measurements. Notably, two distinct procedures occurred in the device when the water droplet contacts with the film. The first procedure is dominated by air-pipe CE (Figure 4a), which means that the water droplet surface is already positively charged once falling through the ambient air or from a pipe.[22] This next step is a conventional CE process, which is similar to the previously mentioned examples.[19,23] In such cases, the PTFE film is initially in electrical equilibrium. As the positively charged water droplet impacts on it, the surface is immediately negatively charged, compensating for the positive droplet under the electrostatic effect. Electrons are drawn from the connected ground to the adjacent electrode following the effect of the Coulomb force. After impaction, the droplet gradually spreads and eventually submerges a larger area of the surface under the influence of gravity, resulting in strengthened attraction toward electrons and sharp enhancement in the magnitude of the current flow. After the droplet deviates from the surface, surface-concentrated electrons lose the potential attraction from the ground and the positively charged liquid. Therefore, the electrons flow back to the ground. The reversible movement generates an alternating current signal, which can be utilized as energy supply or physical sensing.

Another different procedure is dominated by both the water droplet and the surface CE (Figure 4b).[22,24] It is more complicated for the potential construction progress of the surface and the droplet. In the first step, which differs from the air-pipe dominated mode, the very first droplet is at the charge equilibrium state as well as the surface. When the water droplet drops and impacts the electric-neutral surface, a CE process begins by the collision. The process fundamentally follows the typical CE pattern, and the surface and water are charged after contact, respectively. However, the surface remains charged after the positively charged water rolling off, because the PTFE film reserves the triboelectrification charges. The surface starts to be negatively charged after the first impaction, and it is soon compensated for by the positive charges on the electrode implanted in the substrate. If a new droplet subsequently falls on the surface, the cations inside of the water are influenced by the charged surface and redistributed. The attracted cations assemble on the liquid surface and participate in the electrical compensation as well as the positively charged electrodes. With the droplet comprehensively spreading over the film, more cations are concentrated on the contact interface. With the increment of the contact area and the amount of cation in water, the positive charges on

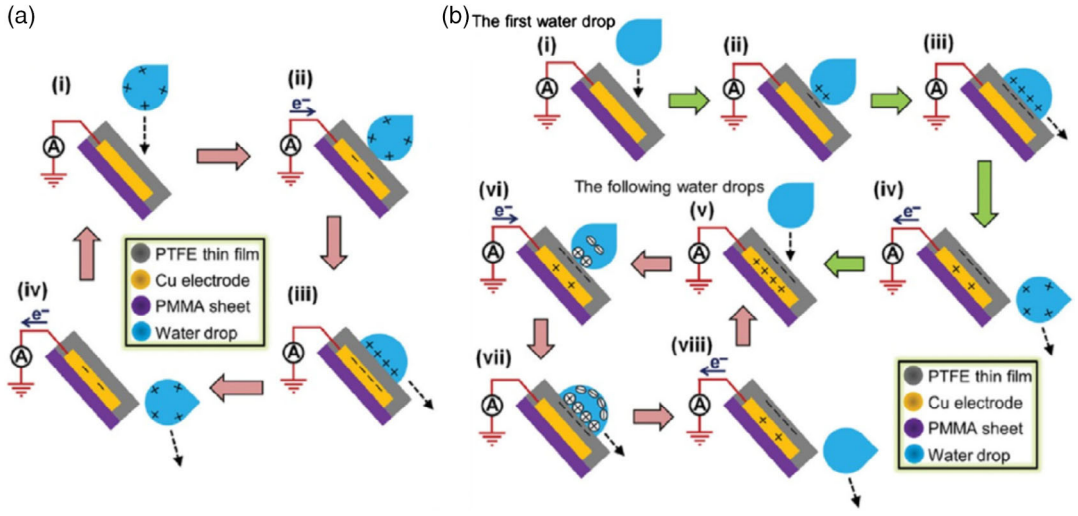

Figure 4. The single-electrode mode of water TENG. a) Water droplet and air-pipe CE dominated electrification processes. b) Water droplet and surface CE dominated electrification processes. Reproduced with permission.[22] Copyright 2014, Wiley VCH.

the electrode are gradually offset. When the surface is fully compensated for by the polarized droplet, the electrode exhibits electric neutrality. The variation of charges on the electrode produces an AC-type current in a connected circuit when the cycling motions proceed. This two-step characteristic creates a different working pattern from the signals generated by two solid objects. Jiang et al. proposed a module by periodically emerging and submerging the TENG device into an aqueous solution.[19] When inserting the device into the oil/water multiphase solution, the signals produced from the solution PTFE and electrode/solution interface exhibit opposite varying tendencies. The featured signals enable a self-powered dual-signal biosensing platform depending on the TENG device. However, the single-electrode mode also has been proved to be one of the most widely modified and adopted modes because of its simplicity and adjustability. In Chung's report,[25] they developed a sprayed-on TENG device taking advantage of a commercial hydrophobic layer. The as-synthesized TENG can create a superhydrophobic surface with a contact angle of over 160°. The output performance can achieve an average positive peak V_{oc} of 13.4 V and I_{cc} of 2.1 μA.

The single-electrode mode has been diversely investigated and applied in multiple energy harvesters and self-powered wearable devices. Due to its abundant choices in materials selection, a stretchable and shape-adaptable liquid-based single-electrode TENG (LS-TENG) has been reported by Wang et al.[26] Long-term stable potassium iodide and glycerol (KI-Gly) is regarded as a durable and safe electrolyte liquid for repetitive motions, such as arm shaking and hand tapping. In another case, a flexible single-electrode TENG is manufactured with MXene/PDMS, which can light up 80 light emitting diodes (LEDs) with periodic hand hammering.[27]

3.2.3. Sliding Free-Standing Mode

Another essential mode of water–solid TENG is the sliding free-standing mode, and it mainly focuses on the sliding motion of the water droplet between two electrons. The displacement current is generated by the varied CE area of the water droplets with the two individual electrodes, as shown in **Figure 5**a.[28]

The device is constituted by water droplets (dark blue), electrodes (red), hydrophobic layer (brown), the dielectric layer (yellow), and the substrate (light blue). In this mode, more electrodes are involved to construct asymmetry distributions of droplets on each adjacent electrode.[8,29] Electrode networks based on this mode are also generally applied in a large number of designs owing to their high-efficiency performance and uniform structures.[30] The surface dielectric material of this device is selected to be poly-4-vinyl phenol (PVP), and it overcomes the obstacles such as short circuit or electron depletion to improve the efficiency. Similar to the single-electrode mode, the collision of the droplet onto the surface results in a charge redistribution on the surface. The electrostatic induction occurs on one side due to the attraction of charged water droplets, followed by the positively charged electrode underneath. Later, an electron transmission is revealed from the positive electrode to the other one due to the potential discrepancy. When the droplet subsequently moves to the other side of the surface, the current is in the opposite direction as well, because the covered range of two electrodes by water is also reversed. A 30 μL water droplet sliding across a pair of electrodes with a width of 7 mm can light up an LED bulb. The V_{oc} and I_{cc} are 3.1 V and 5.3 μA, respectively. The elevated output and multiple functional designs depending on the sliding mode have been studied by some other researchers,[31] and a maximum open-circuit voltage of 46 V can be achieved with an 80 μL water droplet. This method is also proverbially used as wave energy collection devices,[32] where 1.03 mW output power and 7.7% efficiency are fulfilled, respectively. Another integrated device is also exhibited in Figure 5b,[28] and the red-indicated surface is modified with nanowires, which makes water immediately repelled. The electrification is induced by a partially submerged surface and corresponding screen-up effect. When electrode A is submerged by one water droplet, an electron

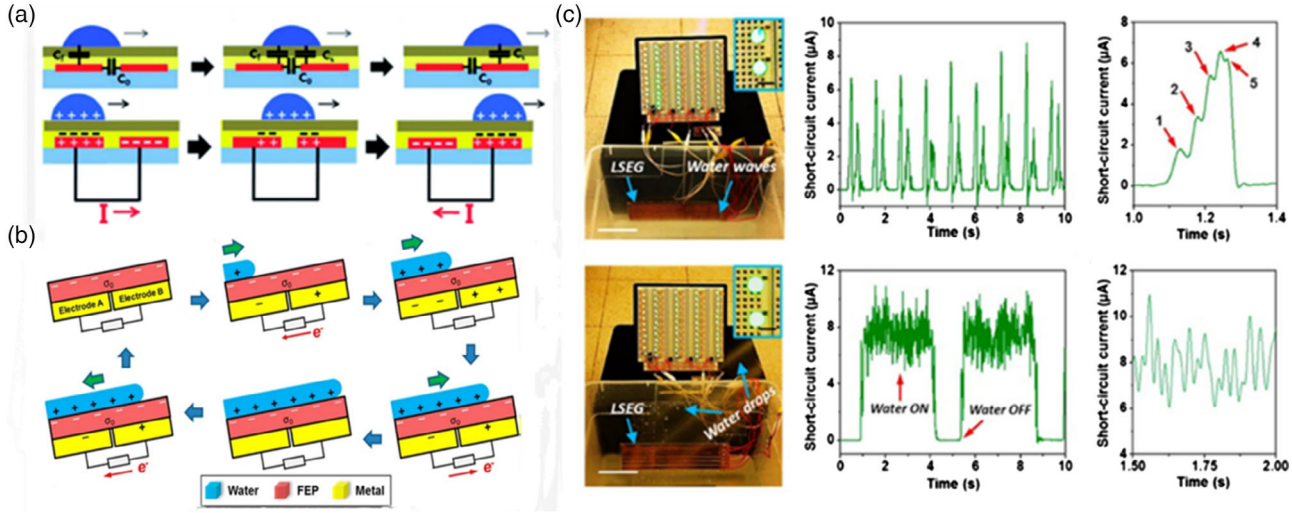

Figure 5. The sliding free-standing mode of water TENG. a) The schematic illustration of work principles. Reproduced with permission.[28] Copyright 2014, Royal Society of Chemistry. b) The sliding free-standing mode with a titled surface. c) Demonstration of the as-fabricated TENG device harvested energy powering bulbs. Reproduced with permission.[32a] Copyright 2014, American Chemical Society.

double layer was composed on the solid–water interface, leading to an unbalanced potential between two electrodes. As the submerged surface of electrode A increasing, more and more electrons are drawn from electrode B to A due to the increased potential difference. The discrepancy of potential gradually decreases, following the water spreading onto the other side electrode, until it fully rolls off. Figure 5c shows a real picture of the experimental setting of the device and its function wave.[32a] The results that assert this kind of practical device are capable of harvesting ambient wave motion, and the generated power can sustainably light a bulb. The device is placed in a water container and titled repeatedly to gain a reciprocating wave. The traveling wave simulates the circumstance around the seashore and produces a current pulse with multiple peaks indicating the wave frequency. The features of response signals reflect the sequential interactions between waves and corresponding reaction units.

Except for the direct impact motion of water droplets, large amounts of devices are also integrated as entirely enclosed structures to overcome the abrasion from straight impaction. A schematic illustration of an enclosed TENG device[33] is exhibited in **Figure 6**a–c to show an experiment picture of the transparent conformation. The water–solid CE phenomenon is produced by a Kapton layer and a nylon ball inside of the circled layers. The two parenthetical electrodes are adherent outside of the Kapton film and connected with the external circuit.

3.2.4. Press-Releasing Mode

The third mode can harvest water motion energy via the hydrophobicity and hydrophilicity characteristics of two different materials. This mode can be driven by any reciprocating motion, which extends the applicability and availability of the devices. Distinct from the single-electrode mode or the sliding free-standing mode, in which water droplet usually impacts or contacts the device surface on one side, the press-releasing mode TENG is composed of two pieces of flats both connected with electrodes, and the liquid is inside of the two flats forming a sandwich structure, as shown in **Figure 7**a.[34]

The method is based on the changes of contact areas of two flats, and electrostatic double layers (EDLs) formed on both sides make two serially connected capacitors. In this mode, water motion is merely required by the electricity generation, because the droplet mainly functions as a resistor. One of the two indium tin oxide (ITO)-coated glass is deposited with PTFE constituting a superhydrophobic surface,[35] and the other one is only coated with conductive ITO to make a hydrophilic layer. While a pressing motion is applied to the flat, the contact area of the top plane increases due to its high affinity to water. Fractional cations in the water move toward the top flat, causing the capacity variation and the potential increase. This cation redistribution has been proved to be the origin of a measurable current signal when pressing the plane. Conversely, if the stress is withdrawn, the sandwiched structure regains the original distance as well as electron transmission. As a result, the inverse current flow is revealed. This device can be driven by any reciprocating triggering, once the relative distance of two components is changed, which is further revealed by the electrical signal. As indicated in Figure 7b, the fundamental circuit simulation of the device is also exhibited.[34] A resistor–capacitor model can be introduced to describe the current flow and voltage variations with the cycling motion. This device can be applied for harvesting sequence motions of walking from a footprint.[36] Krupenkin et al. have achieved a significant power output of 2 W under a 10 V bias voltage by a

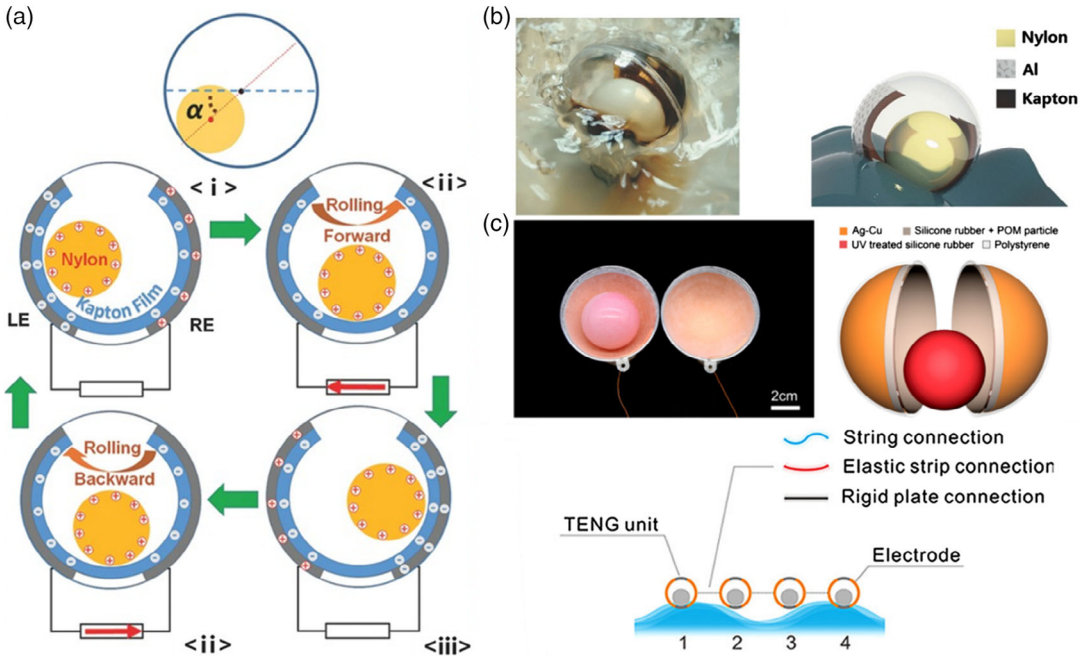

Figure 6. Enclosed sliding free-standing mode. a) Schematic illustration of the enclosed TENG. b) Real photograph of the as-fabricated TENG, Reproduced with permission.[33a] Copyright 2015, Wiley VCH. c) Silicon-based enclosed TENG and design of connection. Reproduced with permission.[33b] Copyright 2018, American Chemical Society.

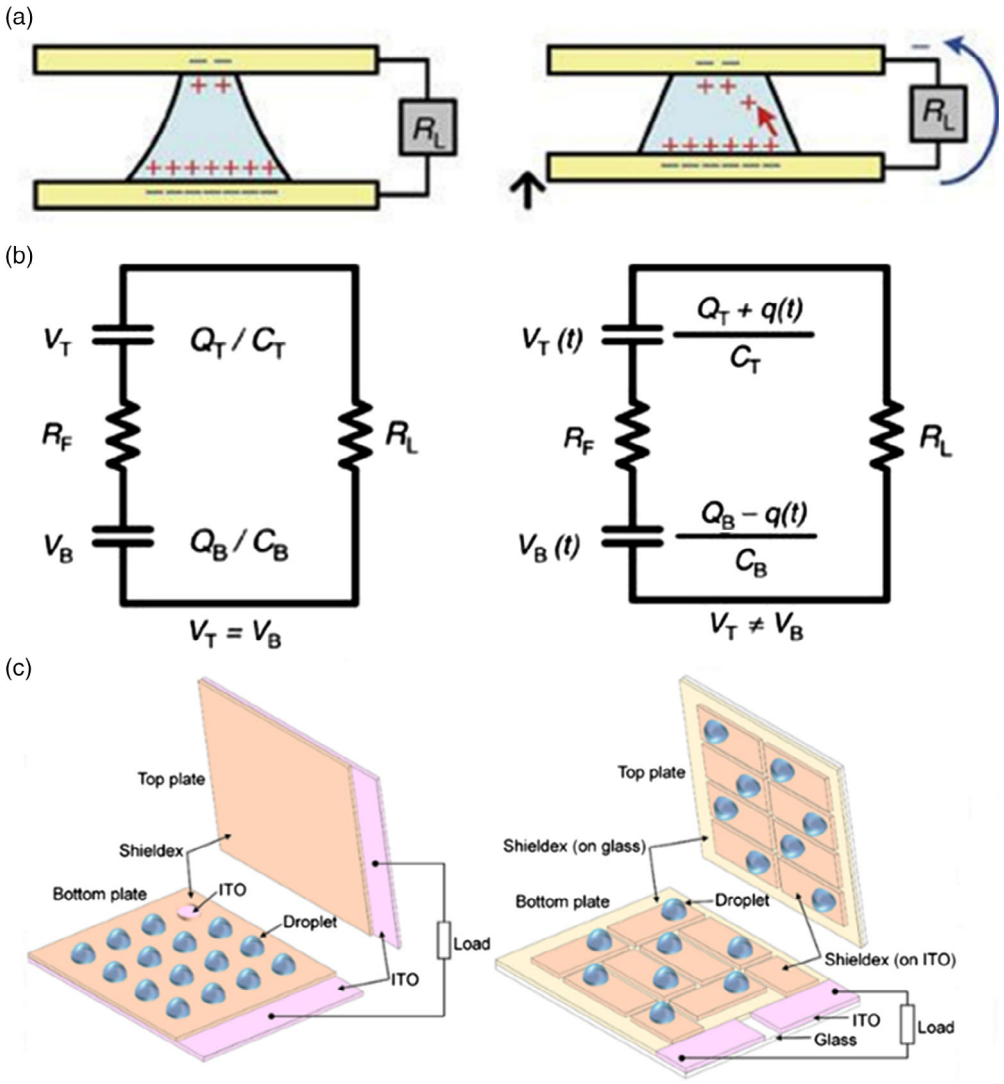

Figure 7. The press-releasing mode. a) The schematic drawing of the pressing status and the releasing status. b) A fundamental circuit simulation of press-releasing mode. Reproduced with permission.[34] Copyright 2013, Springer Nature. c) Schematic of the parallel-droplet and serial-droplet devices based on the press-releasing mode. Reproduced with permission.[37] Copyright 2020, Elsevier.

press-releasing based device with a 40 cm^2surface area. Figure 7c also shows the integration of multiple aligned TENG devices with two pressing flats as the capacitor.[37]

3.3. Streaming Current

Another energy harvesting pathway preliminarily builds on the streaming current, which has attracted a-long-term interest to date from the establishment of the electric double-layer theory.[38] It was first presented by Helmholtz in 1879[38a] and further amended by Gouy and Chapman in 1911–1913.[39] The Gouy–Chapman model indicates that, when a solid is submerged by the liquid or other ionic solution, two layers of charges are formed on the interface (**Figure 8**a,b).[21]

The inner layer is normally acknowledged as the Stern layer,[40] which is typically formed by ions adsorbed on the solid–liquid interface constructing a compact layer. The outer layer is named the diffuse layer, which is composed of mobile counter ions. These ions are loosely bound to the surface and driven by the liquid flow. An external pressure difference or concentration difference can influence the liquid flow, producing an electrical current due to the charge immigration phenomenon. This ion flow is proved to be the streaming current.[41] With nanoscale fabrication and detection emerging, streaming current phenomenon was further developed by Stein and co-workers.[42] A schematic illustration of the EDL in an as-fabricated silicon channel and streaming current driven by air pressure is depicted in **Figure 9**a.[42]

Microfluidic generators with diverse function modes are fabricated, relying on the principle of streaming current. They are favored in self-powered systems because of the excessively high adaptability. The device outputs a constant current of 10 pA with the ionic solution with a low salt concentration, however, increasing the solution concentration causes a current decline. Another

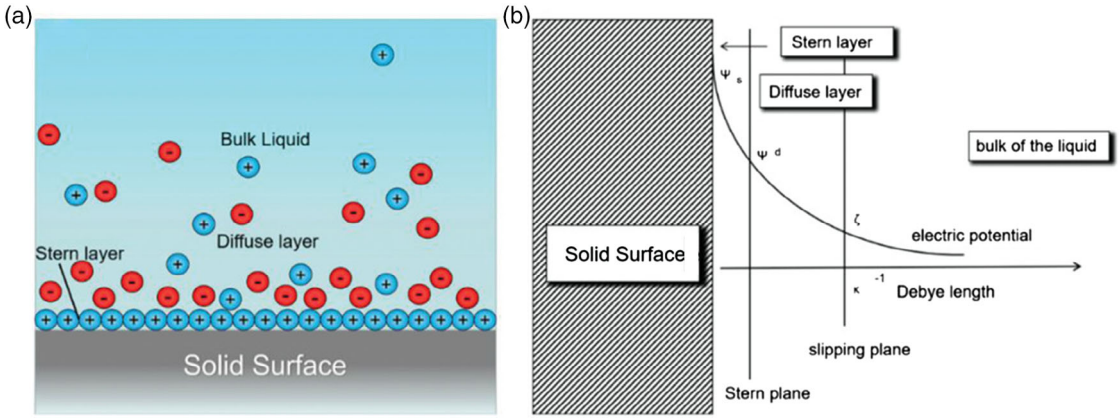

Figure 8. a) The schematic of the water–solid interface. b) The electric double layer. Reproduced with permission.[21] Copyright 2019, Wiley VCH.

study proposed by Zhang et al.[43] used a macroscopic channel and porous surface materials to enhance the sensibility (Figure 9b). By utilizing the potassium chloride (KCl) solution, this device can yield a larger output current of 1.75 nA. Except for functioning within the channel structure, the report also stated that[44] the streaming current effect was also available when implementing on thin films such as polymer[45c] and graphite.[45] With the rapid advancing of fabrication and modification, the power generation performance can achieve a 1.65 mA current with a voltage of about 150 mV, respectively.[46] In addition, the electrification phenomenon can also emerge when altering the potentials of EDL in drawing or waving mode as in Figure 9c,d.[47] The device can sufficiently support the self-powered devices for its stable performance during the electricity generation process. This discovery also benefits the device fabrication progresses, because the TENG based on streaming current typically has small size and simple conformation. This device can output a continuous direct current and be used as a power source without rectifier or storage components.

3.4. Hybridized Mode

Although EMGs are typically considered as complicated and heavy equipment, hence, they are infeasible to broadly apply for large-scale energy harvesting. Hybridized with TENGs can improve flexibility and enlarge the choice of materials, therefore reducing both cost and consumed time. A hybridized spherical device was synthesized and analyzed for its prompt response to excitations from any orientation. This hybrid triboelectric–electromagnetic water wave energy harvester (WWEH) consists of three sections: a TENG module, an EMG module, and the rectifier circuits. These three sections are all packed inside of a layered spherical shell. The functional part of each module is divided into three spaces from top to bottom, and the last two sections are linked by the magnetic sphere in the EMG section and the magnetic cylinder in the TENG module. According to the assessments based on Maxwell 14.0 and COMSOL Multiphysics 5.3, the authors revealed the mechanisms and output voltage distributions of this hybrid device. The WWEH is designed for placing on the flotation device, such as buoys, spars, and so on. When excited by the water wave, the magnet inside of the WWEH rolls, and the mover slides on the friction layer under the attractive force between the sphere and the cylinder. With an integrated rectifier bridge, the TENG and the EMG modules are connected in series to function as a charge generation and storage system. The output performance is highly correlated with the frequency and the angle of inclination, and the maximum voltage reaches 172.95 V_{pp} with 135° at 30 rpm. The verification experiment in Lake Lanier also elucidates the device, which can produce 1.69 mJ electrical energy with 162 s.

The other team also reported a novel hybridized design that shows great advantages when operates in the low-frequency range (<1.8 Hz). The TENG section of this device was made of a group of rolling aluminum rods and PTGE-coated electrodes, and the EMG section was composited with six pairs of square magnets. The relative movements between magnets can drive the rolling of aluminum rods, which rendered a sufficient and sustainable method toward hydropower harvesting by low-frequency triggering.[48]

4. Affecting Parameters

4.1. Morphology and Surface Parameter

The aforementioned water-solid CE modes mainly focus on the fundamental interactions that emerged on the interface. However, surface properties highly affect the eventual output performance with complex influences. The water–solid interface is well known for the double-layer structure, and the two charge layers make the friction on the interface different from that of solid–solid pairs. Surface morphology is an essential factor altering the contact condition by changing the contact area and compaction. Micro/nanoscale roughness of the solid surface can significantly increase the output performance with other properties remaining consistent. There are two different origins for explaining the enhancement: 1) improved surface hydrophobicity accomplishes less friction on the interface and 2) improved surface contact area induces a larger electrification effect. Due to the existence of Cassie's law, surface roughness can improve the hydrophobicity of a surface and increase the water spreading

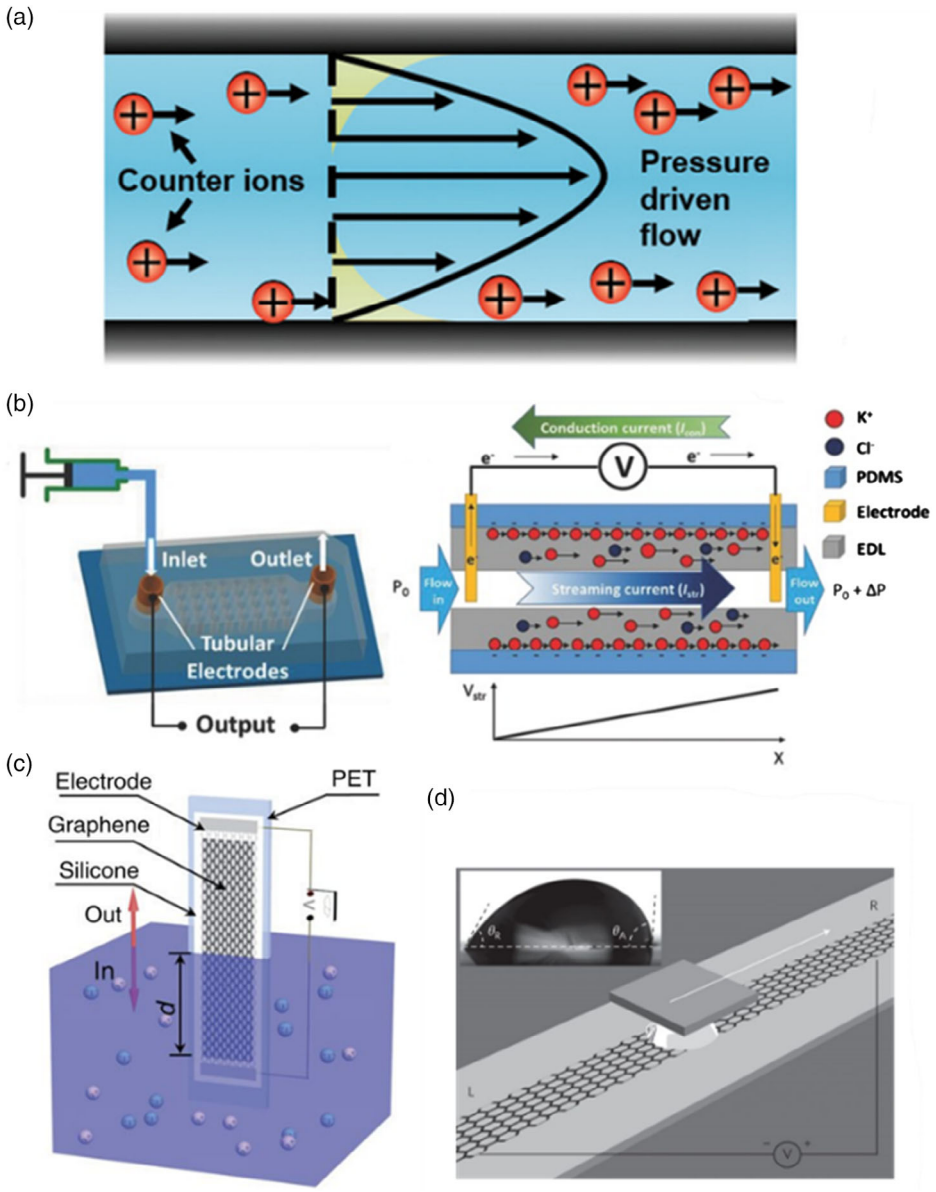

Figure 9. a) Electron double layer and pressure-driven streaming flow. Reproduced with permission.[42] Copyright 2005, American Physical Society. b) A streaming current generator. Reproduced with permission.[43] Copyright 2015, Wiley-VCH. c) Drawing mode. Reproduced with permission.[48b] Copyright 2014, Springer Nature. d) Waving mode. Reproduced with permission.[48a] Copyright 2014, Springer Nature.

speed.[49] A large reduction of the contact area in hierarchically structured surfaces[50] and a simultaneous decrease in contact friction effect have been demonstrated (**Figure 10**a–c).[51]

4.2. Water Property

Lun et al. implemented a series of examines for assessing massive kinds of liquids and ionic-composed solutions for their triboelectrification performance, revealed the correlations between liquid characteristics and TENG performances. They preliminarily utilized six kinds of different type of liquids for the rotary tubular TENG device.[52] The TENG device was operated with a consistent parameter in both surface contact area and roughness, and the output performance was only affected by the liquid inherent properties. Based on the examination, the voltage of hexane, isopropanol, and ethanol was relatively low in all six samples, especially when compared with DI water. While it came to acetone and ethylene glycol, the voltage slightly increased but still less than that of DI water. In another work,[53] five more liquids were co-tested with the previously introduced six liquids, which were ether, chlorobenzene, *N,N*-dimethylformamide, acetonitrile, and dimethyl sulfoxide (DMSO). Among the two experiments, DI water both exhibited the highest output voltage. In the U-tube TENG model,[53] the voltage V can be estimated by

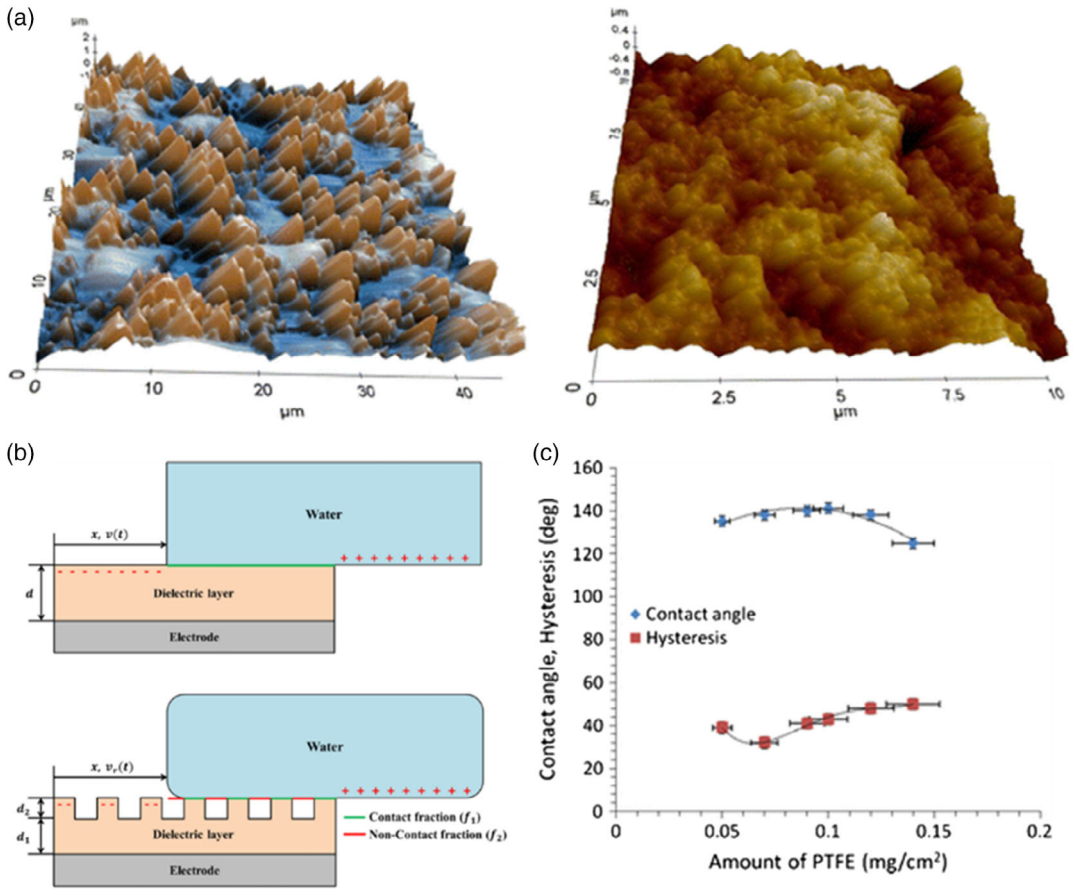

Figure 10. a) 3D AFM topography of laser textured silicon surface and Teflon deposited surface. Reproduced with permission.[53a] Copyright 2012, Springer-Verlag. b) Theoretical model for a flat surface and modified rough surface. Reproduced with permission.[53b] Copyright 2018, Elsevier. c) Hydrophobicity of as-deposited surface in terms of static contact angles and contact angle hysteresis. Reproduced with permission.[53a] Copyright 2012, Springer-Verlag.

$$V = \sigma\omega\upsilon Rln\left(\frac{l - \upsilon t}{l}\right) \tag{1}$$

where σ represents the triboelectric surface density, and ω, υ, and l are the dielectric parameters and fixed in a certain TENG device. Thus, σ is the most crucial parameter for evaluating the device output and highly related to the liquid inherent properties. The polarity and contact angle are also presented in **Figure 11**a[54] and show a positive correlation with the generated voltage. These parameters compose a complicated co-effect on the device output. For instance, 2-ether generally presents an impartial voltage output when compared with 1-hexane. However, its polarity is much higher than that of 1-hexane. This is for the adverse effect induced by the lower contact angle of 2-ether. It gives an insightful perspective about the interferes of parameters in liquids, demonstrating output is positively correlated with polarity, dielectric constant, and the affinity to fluorinated ethylene propylene (FEP).

Except diverse liquids have been used as alternative dielectric materials, and solutions with the distinctive types of ions are also desirable and momentous in water–solid TENG manufacturing. The type and concentrations of ions are both essential aspects of power generation due to different circumstances as harvesting energy in the forms of ocean waves, droplets, and river flows. The appearance of multifunctional TENG devices also provides a nondestructive and highly flexible method for microliter sampling and simultaneously sensing. For demonstrating the influences of ionic additions, a comprehensive investigation based on distinctive solutions has been conducted with a single-electrode mode device. Standard solutions with different ions[53,55] are shown in Figure 11b. The experiment shows that the electrical conductivity (κ) has a positive correlation with the reciprocal of the output signals I_{sc}, V_{oc}, and Q_{sc}. With the high sensibility to ionic solutions, the TENG can be utilized as an active micro-liquid concentration sensor with identical and selectable output signals, such as I_{sc}, $V_{oc,}$ and Q_{sc}.

The open-circuit voltage and short-circuit current were detected, respectively. Various performances of different solutions were also illustrated, indicating multiple factors attribute to the output.[31a,53] The effects of ionic aqueous solutions generally rely on the interactions between free ions and surface materials. Previous studies revealed two fundamental reasons influencing triboelectrification on water–solid TENG devices with ionic aqueous solutions: 1) the electronegativity of the ions, which reduces the potential differences by screening up the

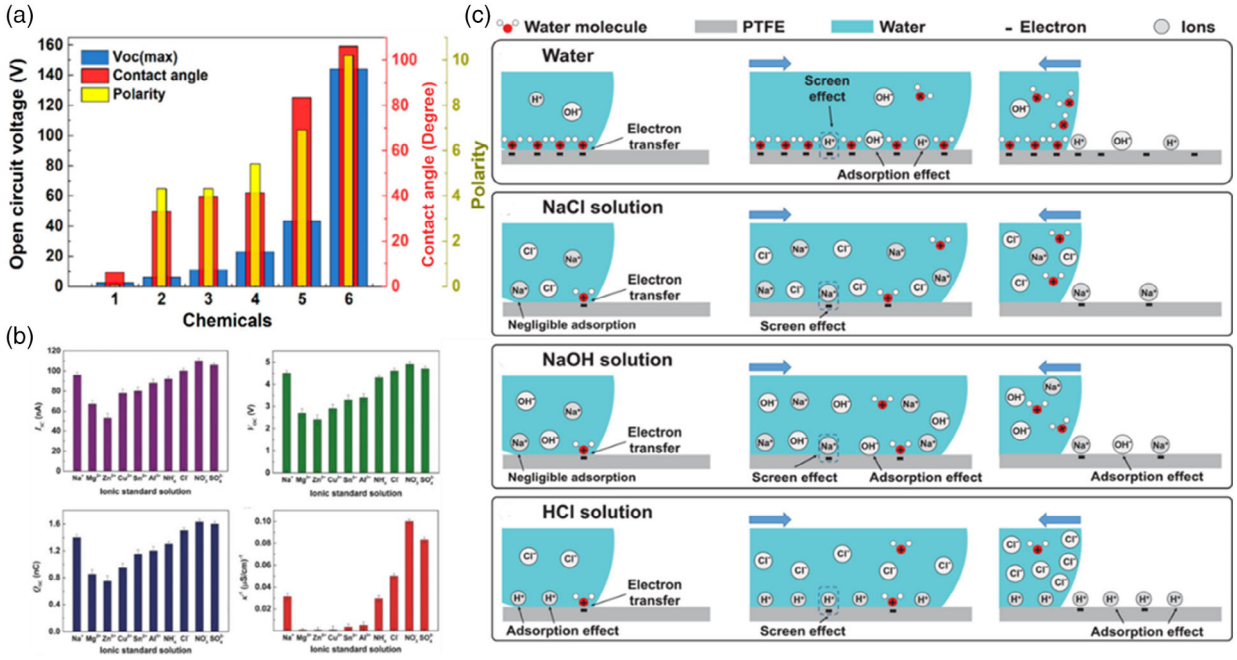

Figure 11. a) Relationship between V_{oc} and contact angle and polarity for the measured liquids (1—hexane, 2—isopropanol, 3—ethanol, 4—acetone, 5—ethylene glycol, and 6—DI water). Reproduced with permission.[54] Copyright 2019, American Chemical Society. b) The concentration influences of Ionic solutions indicated as outputs I_{sc}, V_{oc}, Q_{sc}, and electrical conductivity. Reproduced with permission.[55] Copyright 2017, Wiley VCH. c) Mechanism of CE between different ionic solutions and PTFE film. Reproduced with permission.[11] Copyright 2020, Wiley VCH.

electrification electrons on the interface. The ions with low electronegativity are intended to absorb the F^- groups on the typical surface materials, such as FEP or PTFE, hindering the output performance. 2) The conductivity of the ions, which declines the generation of negative charges on the surface because of the ions attracted by tribo-charges leading to reduced output. For clarification, when the CE occurs on the interface, tribo-charges are generated and preliminary distributed loosely on the surface. Owing to the existence of a high concentration of ions in the solution, the interface potential difference is reduced by ion absorption, and fractional generated electrons are compensated for by diffusing cations in the liquids. This would cause a total inferior output performance of the TENG device.[31a,53] Figure 11c shows the schematic processes of triboelectrification with or without the existence of ions.[11] The addition of ions leads to massive free ions in the aqueous solutions, results in a decrease in interface charge transfer due to the screen effect. Except for the ionic aqueous solutions and different liquids, the droplet volume, initial height, and tilting angles would also cause enormous variations on the device performances.

The pH value is also an important characteristic of water, which is rarely to be neutral in natural environments. Researchers have reported several pH detectors based on output voltage differences with TENGs.[56] The results indicate that similar decreasing trends have been obtained both when the pH value changing from 7.0 to 2.0 and 7.0 to 11.0. As the solution contains more H^+, the cations in the electrolyte solution can be rendered by abundant H^+, leading to the concentration reduction of triboelectric charges.[56] OH^- also shows a compatible influence on the output voltage in a SiO_2-based TENG device. The report shows that the decay of the SiO_2 surface charge density is originated from the O^- ions increment assisted by OH^-. When pH increased to 11.0, the electron transfers have strongly deteriorated, and ion density was higher than that of DI water. However, the overall charge transfer was reduced.

5. Energy Source

Multiple designs and modifications have been introduced in different modes of TENGs for harvesting hydropower in nature. It emerges in the forms of ocean waves, river flows, raindrops, floods, and other arbitrary mechanical movements. The specification and adaptation of the device are vital for versatile applications.

5.1. Water Waves Energy Harvesting with TENG

The past short lustrum has witnessed lots of water-TENG devices invented for creating a novel sustainable energy source.[31a,57] Blue energy is abundant on the earth but mostly squandered for the technical encumbrances, which requires a flexible and decent generator. TENG devices with sliding free-standing and contact-separation modes are most commonly used for the energy conversion in water, and some of the designs and fabrications are shown in **Figure 12**.[32b,58]

Figure 12a shows a network-shaped sliding free-standing TENG device for energy harvesting.[32b] A highly adaptive design enables practical applications in real circumstances. Owing to the uncontrollability and unpredictability of water, this device can transform the unstable triggering to a constant output,

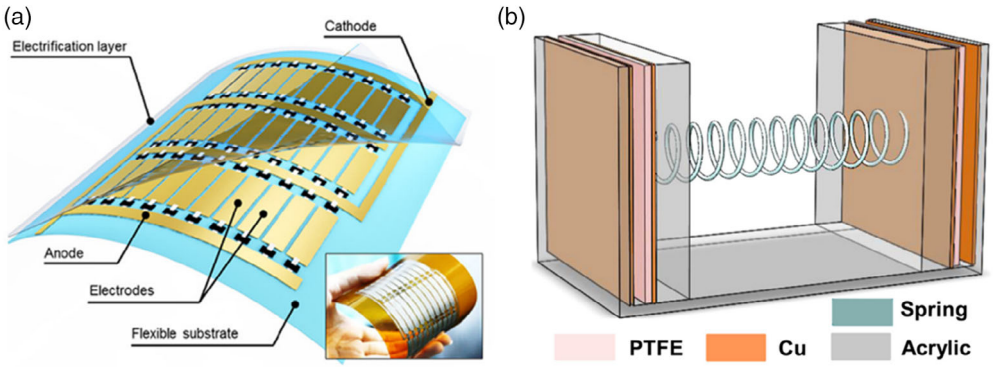

Figure 12. a) Structure of a networked integrated TENG. Reproduced with permission.[32b] Copyright 2018, American Chemical Society. b) Schematic illustration of the spring-assisted TENG structure. Reproduced with permission.[58] Copyright 2017, Elsevier.

sufficiently functions as the energy supply for self-powered wireless systems. It produces an unbalanced potential distribution between two electrode columns when the water wave vibrates. However, previous TENGs were only effective with regular water motions, which can interact with the surface in a linear direction. As indicated in the figure, multiple pairs of electrodes are aligned on the surface of the flexible insulator material. The scale of the device was 100 mm in length and 70 mm in width; however, the output performance can achieve 1.03 MW when applying a 22 MΩ load resistance. The high-efficiency and small-scale characteristics make it a great pathway for energy harvesting in complex conditions. It has been demonstrated that the 2D arrayed electrode network can sufficiently suppress the conversion efficiency reduction, because this kind of structure is hardly affected by the random motion of water waves. Another model was constituted as an enclosed structure based on the CE mode (Figure 12b),[58] and all electrodes and contact materials were sealed inside of an acrylic box, which was apparently insulated and inflexible. The two copper electrodes were fixed on the opposite inner walls of the box, respectively. In the middle of the box, two acrylic blocks were tightly attached to the isolated electrodes with a layer of PTFE on the contact surface. The iron spring connected to the back of two blocks was utilized to make a firm and complete contact when the device shaking with the wave motion. After the electron-injection modification, the TENG device could induce a larger output performance when operated with a higher material surface charge density. The mechanism of the device is similar to a conventional contact-separation mode as mentioned in the previous section. When the water collides on the box TENG, components inside of the box change the relative positions in accordance with the inertia effect. The PTFE layer on the acrylic block surface compacts on the Cu electrode surface and makes the Cu electrode positively charged and the PTFE negatively charged in the compacted side, and a current is generated. With the periodic movement of the spring, an alternating current is produced. The model indicates the potential applications of enclosed independent devices in the oceans.

5.2. Flowing Stream Energy Harvesting with TENG

The marine environment is described as powerful wave motions with high frequencies and large quantities. The flowing stream is another common type of water kinetic energy, and the recent investigations also put forward disparate concepts for TENG development. Rivers and pipe flows are the typical forms of flowing stream,[59] and the traditional way to facilitate the energy over a river stream is mainly based on electromagnetic effect. However, triboelectrification-based energy conversion can be applied in circumstances, which have a slow motion. **Figure 13**a–d presents a highly transparent triboelectrification nanogenerator based on the single-electrode mode.[58c] It utilizes conventional organic materials and makes the fabrication of the device less influenced by the constituent limitation. The top and bottom layers of the device are composed of polyethylene terephthalate (PET) and bent to the same degree. Both flats package a copper electrode and a layer of PTFE inside on the camber. PTFE nanowire arrays are deposited on the copper electrode contacting with the middle Al plate, which can enhance the charge density of triboelectrification. The device can obtain an average output power of 1.15 MW with 1 km^2surface area, given its low cost and simple structures, and this device provides a promising outlook for large-scale water energy harvesting. Although river streams are abundantly available, the applications generally lack decent study and consideration. Figure 13e shows a hybridized wheel-type TENG for harvesting both the kinetic energy and electrostatic energy contained in the river flowing streams. The device is constructed with eight blades surrounding a plate, and the surface of the blades is attached with PTFE to form a classic single-electrode system.[60a] The water flows and impacts the surface and bounces off and makes individual PTFE blade function as a single-electrode water-TENG device. Moreover, the whole device is a hybridized equipment constructed by a water–solid TENG and a solid–solid TENG. The central part is composed of two similar flakes, and the collision induced by flowing water can emerge the relative displacement between two flakes; then, it operates as a solid–solid TENG. The device can obtain an output voltage of 75 V and a current of 12.9 μA, respectively. This kind of hybridized fabrication can simultaneously harvest two types of energy contained in water flowing with a small flowing rate.

5.3. Raindrops Energy Harvesting with TENG

The raindrops are also inclined to be ignored in daily life, because the practical inventions based on raindrop are

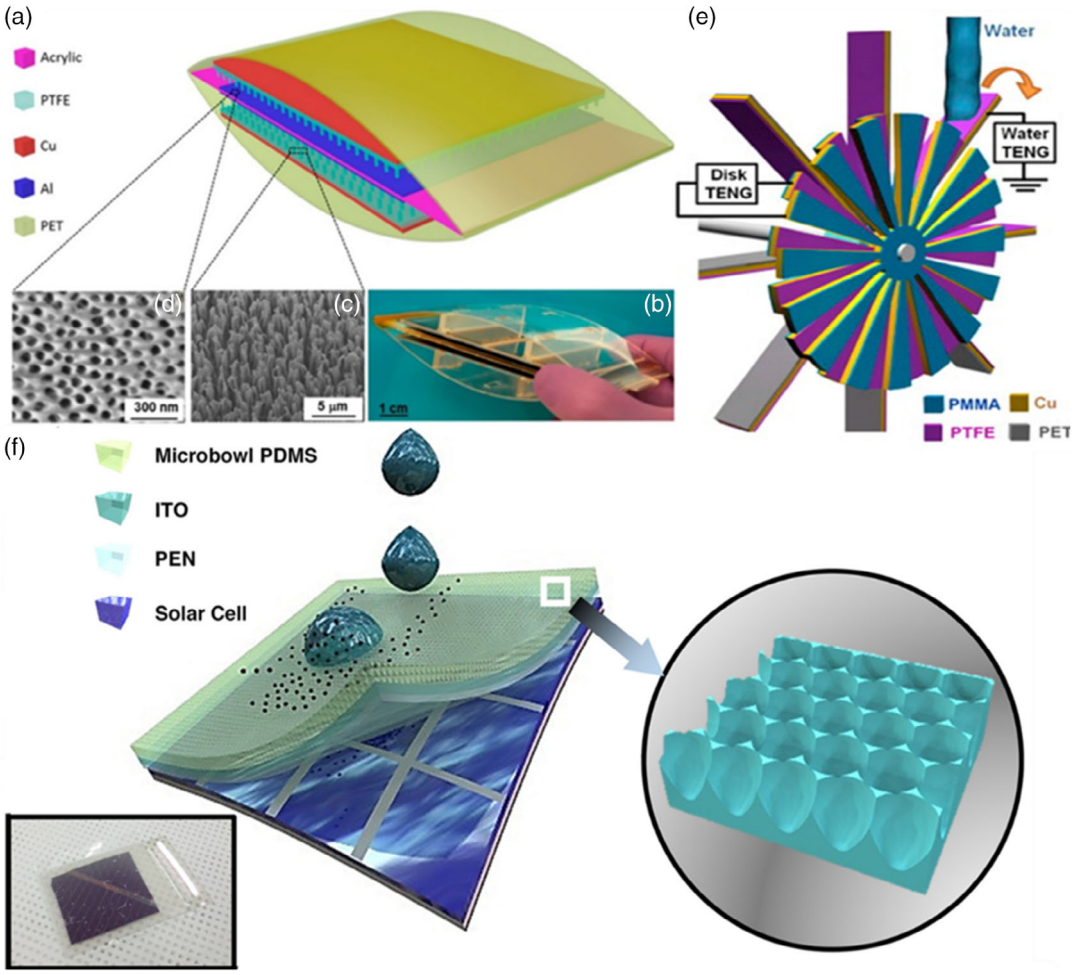

Figure 13. The multiple types of designed TENG for harvesting streaming and raindrop energy. a) Schematic illustration and b) photograph of an as-fabricated device. c) SEM image of PTFE nanowires. d) SEM image of nanopores on the aluminum electrode. Reproduced with permission.[58c] Copyright 2015, American Chemical Society. e) Schematic illustration of a wheel-type TENG. Reproduced with permission.[60a] Copyright 2014, American Chemical Society. f) Schematic of the hybrid cell for collecting solar energy and raindrop energy. The inset shows a digital photograph of the surface micro-bowl structure and a real photograph in the experiment. Reproduced with permission.[62c] Copyright 2015, Elsevier.

excessively limited by materials and environmental factors.[29b,60] However, rain is the well-known universal climate, which occurs around the world and has the advantages of continuous motions and large quantity. This leads to an excellent potential strategy for renewable and sustainable energy supply. The conventional designs for harvesting raindrop energy are designed in the single-electrode or sliding free-standing mode, and the reason is that raindrops loosely diffused in the ambient and hard to be collected in contact mode. The common fabrications of the raindrop harvester are typically on the umbrella and the outside of a building, which have a strong probability of contacting raindrops. The integration with a solar cell for harvesting the energy from sunlight and raindrops at the same time also emerges.[61]

Figure 13f presents a hybrid cell for simultaneously converting solar energy and water energy.[62] Hybrid cells are typically difficult to fabricate for practical use because of their complicated structures and high cost. This hybrid TENG energy-harvesting device is based on the CE effect and a conventional solar cell. The surface configuration is specifically constructed for raindrops impaction, but also capable of solar energy absorption. It is noteworthy that the surface material overcomes the power degradation effect, because airborne dust contamination can be sufficiently washed away by the impacted raindrops. As we illustrate in the former section, the surface properties are essential for the overall performance of the TENG device; thus, the surface plane is normally engineered with hydrophobic materials.[19,25,35] Due to the surface characteristics, water can be easily removed from the functional section of a TENG device and simultaneously bring the dust away. In the contrast, if the particle cannot be washed away by this water motion and instead of sticking on the surface, the output performance can be degraded for both the obstruction of dust and contact area reduction. By the self-cleaning effect of the device, a high level of immunity against the dust residue can be achieved. The fundamental structure of the hybrid cell is anchoring a transparent water-TENG device on the surface of a conventional solar cell. The transparency of the surface material is for the absorption of the photon energy, as the solar cell is embedded under the TENG. The device is

fabricated with a layer of PDMS and a micro-bowl array on an ITO/polyethylene naphthalate (ITO/PEN) subtract. This top layer functions as a single-electrode TENG, and the solar plane works for harvesting the light energy. It produces a more consistent energy output in actual conditions. This as-fabricated device accomplishes an output voltage of 7 V and a current of 128 nA with the untreated water droplet. If the device purely works under sunlight, the output performance can reach the level of 0.6 V. While it is driven by the periodic water droplets, the output has a steep increase to 2.7 V. The hybrid cell also shows a high-efficiency recovery rate of 84%, because the two individual energy harvesting processes can be processed without cross effect. However, the experimental examination based on real raindrops suggests that the output performance is highly degraded when ion concentration increases. The advent of this hybrid design still supports the great possibility of multifunctional devices.

6. Application: Self-Powered Sensor

Except for energy harvesting and storage, the TENG device is also capable of sensing and detecting owing to its simultaneous reaction to the environmental variation. The rapid development of industry and information technology has created an extensive driving force for the development of sensors. The growing demands for wireless, sustainable, and portable sensor networks are desirable. TENGs are typically investigated for the renewable energy supply; however, the working mechanism is advanced of real-time response, making it a promising strategy for self-powered sensing. A group of self-powered sensors has been invented for, e.g., mechanical motions,[62] the contact pressure of a water droplet,[62] and biological movements.[63] In this section, several devices focused on self-powered sensors are asserted and explicated.

6.1. Mechanical Motions

Tactile/touch sensor[64] is generally utilized for measuring information induced by physical interactions between the device and the ambient environment. According to the transducing mechanism, the tactile sensors can be divided into typical categories, such as capacitive, piezoelectric, or optical. The mechanisms of tactile/touch sensors generally depend on the deformation of the sensing constituents when interacts with an external force. It imposes a great challenge when operates with excessively low pressure. However, the unconventional sensing mechanism of the triboelectrification-based sensor enables exceptional pressure sensitivity. It is significant for developing human–machine interfacing and innovative materials such as electronic skins or anti-counterfeiting inks.

A self-powered TENG sensor is schematically shown in **Figure 14**a,[65] and this device yields a voltage signal as a real-time response for external physical triggering on the contact sensing surface. A layer of PET constitutes the substrate of the self-powered triboelectric sensor (TES), while both sides of the substrate are deposited with a layer of ITO electrodes. On the top plane, an FEP layer is modified as the tribo-functional layer for enhancing the charge production. For further improving the surface sensitivity, vertically aligned polymer nanowires (PNWs) are constituted on the FEP surface to increase the effective contact area (Figure 14b,c).[65] The diameter and length of the PNWs are 150 nm and 1.5 μm, respectively. The self-powered TENG functions in a conventional contact-separation mode, as the tactile/touch motion presents a periodical pattern. The negative charge affinity of FEP materials has been elucidated to be one of the most excellent. With a series of contact-separation movements, the remaining electrons on the FEP surface induce an electric field between two ITO electrodes. Considering the distance differences from the FEP layer to the two different electrodes, the electric potential between the two electrodes exhibits a discrepancy in magnitude. Because the electrodes load an external electrical measurement system, the potential between two electrodes creates an open-circuit voltage difference, and it can be defined as a criterion for estimating the applied force. For instance, when an applied pressure in a scale of 0.03 KPa, the self-powered sensor generates a square-wave output with a maximum amplitude of 35 V. Owing to the micro- and nanoscale surface asperities, the PNWs provide great enhancement of sensitivity in a low-pressure region. This device shows the superior performance of the pressure sensitivity of 44 mV Pa^{-1} (0.09% Pa^{-1}) and the maximum touch sensitivity of 1.1 V Pa^{-1} (2.3% Pa^{-1}) in the extremely low-pressure region (<0.15 KPa) with the surface modification method. Figure 14d also introduces another type of TENG energy harvester and self-powered sensor that is manufactured as a duck shape.[29a] The device relies on the free-standing mode, and the vibration frequency can be detected by measuring the output voltage and current. From an innovation point of view, triboelectrification is universally applicable with many materials; thus, the device can be used without limitations for satisfying different circumstances. However, this device shows not only effective touch sensibility but also a high level of stability and durability.

Despite the plentiful designs and fabrication methods reported in the last decades, researchers are still working industriously on the more materials excellent in manufacture and performance. The sensitivity and productivity are extremely crucial for the practical application of the mechanical sensor. Laser-assisted 2D transition metal dichalcogenide (TMDC) is currently regarded as a multifunctional flexible material with great promise. Recently, a surface-rumpled 2D MoS_2 TENG device has been developed by simple laser-directed thermolysis.[66] In this work, the researchers presented a flexible method for developing flat and crumpled MoS_2 by adjusting the fluence level. The $(NH4)_2MoS_2$ is capable of high optical absorptivity and easily transferred to the 2D MoS_2 layer under the fluence level from 2.52 to 2.61 J cm^{-2}. Once the irradiation fluence is higher than 2.61 J cm^{-2}, the MoS_2 starts to exhibit a crumpled morphology with 3D distortion. The special surface characteristics not only improve the contact area but also cause shear friction, resulting in 40% output improvement than that of flat MoS_2. The crumpled MoS_2 TENG generates an energy output of 25 V, 1.2 μA, and 2.25 μW, which allows the application of a self-powered touch sensor with multitouch and position-mapping capabilities. A 4 × 4 patterned crumpled MoS_2 array was synthesized and transferred to a flexible elastomer substrate, and electrode lines were embedded with an inkjet printer. A connector was linked to the electrode bottom to measure voltage signal

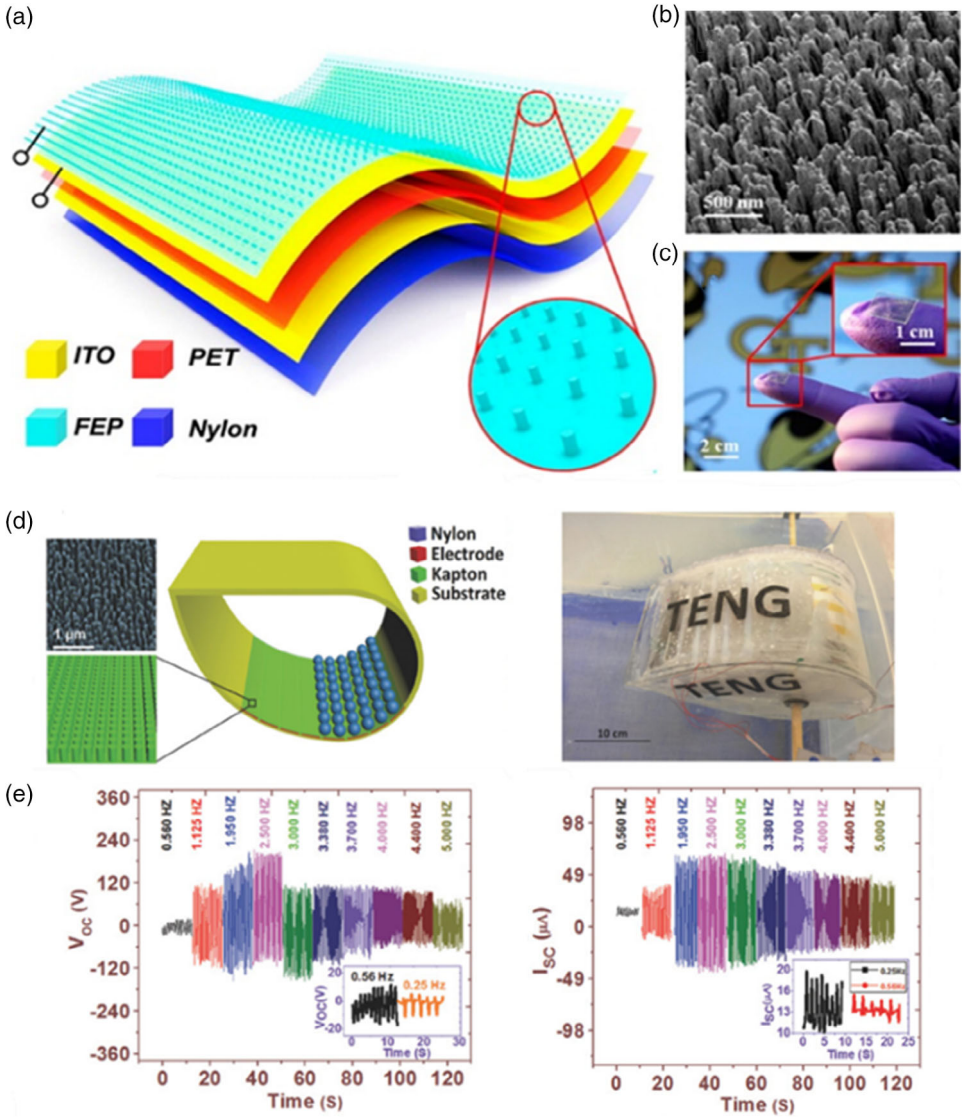

Figure 14. Structural design of the self-powered TES. a) Schematic drawing of the device. Inset shows an enlarged scheme of PNWs. b) SEM image of PNWs. c) Photograph of an as-fabricated TES. Reproduced with permission.[65] Copyright 2014, American Chemical Society. d) Schematic configuration and optical image of a duck-shaped energy harvester based on rolling contact. e) The output performance. Reproduced with permission.[29a] Copyright 2017, Wiley VCH.

changes when touched with a stylus pen. The output voltage of the touch pixel reached 8 V, and the previously touched pixel reached 6 V. The untouched surface can only show a voltage less than 0.8 V. The test was operated with various pressure from 5 to 20 N, and the difference in potential between touched and untouched pixels can indicate the instantaneous position mapping of the trajectory of the pen movements.

6.2. Chemical Motions

Monitoring ambient chemical variation is crucial for environmental safety monitoring and professional healthcare works.[62,67] Except for mechanical monitoring, the chemical sensing equipment has also been investigated for detecting various types of elements in the ambient condition, for example, NH_3,[68] Hg,[36b] and ethanol.[69] In TENG chemical sensor designs, the output signal is based on the type and concentration of target molecules absorbed on surfaces. The differentiated absorption events lead to an output signal variation, which has been widely applied for fabricating biochemical and chemical sensors. As in the aforementioned section, TENG can produce different electrical signals by changing the type and concentration of the ions in water. The conventional triboelectric fluid sensor needs the reciprocal contact-separation events between the liquid; however, materials with low surface energy cannot provide sufficient sensitivity and durability. Herein, a simple triboelectric microfluidic system (M-TENS) has been investigated for rapid and flexible self-powered liquid sensing (**Figure 15**a,b).[70]

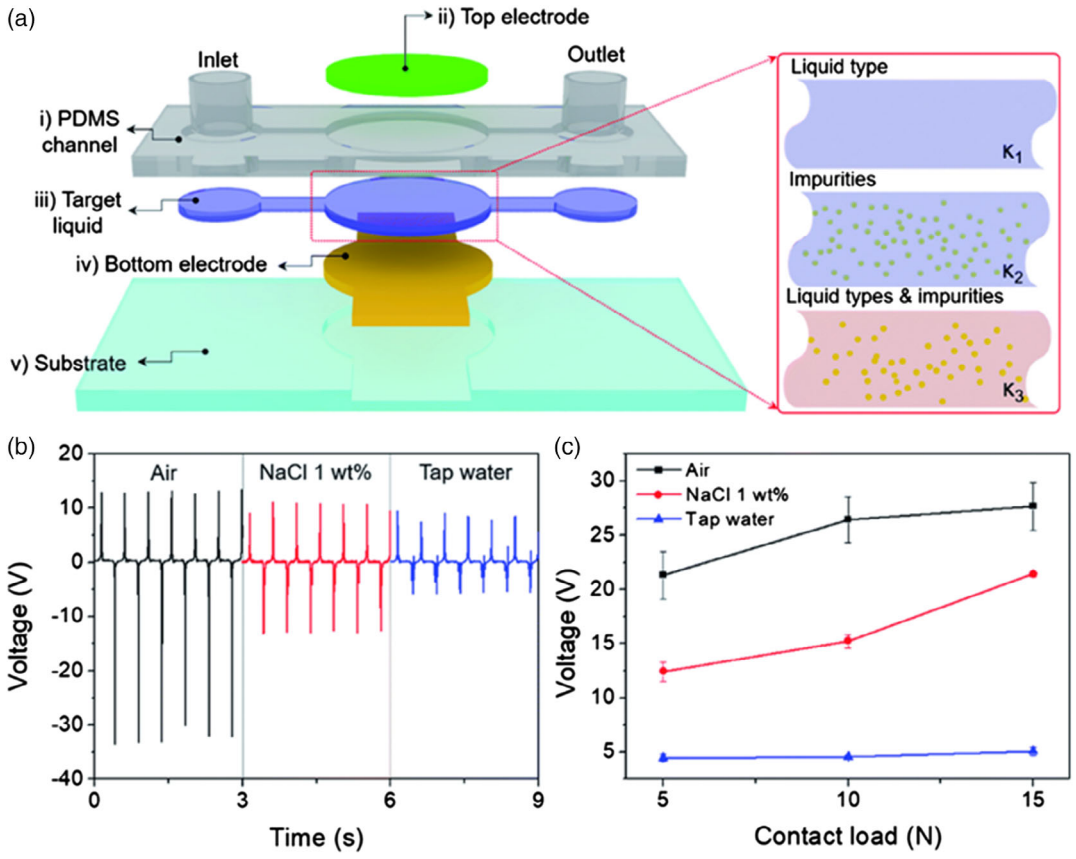

Figure 15. A self-powered triboelectric microfluidic system for sensing ions in fluids. a) 3D schematic of a microfluidic system-based TENG. b) Measured voltages with different fluids. c) Contact load dependency of M-TENS. Reproduced with permission.[70] Copyright 2018, The Royal Society of Chemistry.

The fundamental structure of this device is the PDMS microfluidic channel clamped by two electrodes. When the top electrode is released and separated from the top layer of the PDMS channel, residual ions in the liquid can disturb the charge migration, leading to an output energy drop.[70] According to the experimental results, the output voltage increases with the applied force (Figure 15c), indicating a typically TENG behavior. By varying the fluids in the channel, the output performance achieved a maximum value with an air-filled M-TENS. If the channel was filled with tap water or 1 wt% NaCl solution, the output voltage excessively dropped by about 2.5- and 5.5-fold, respectively. It manifests that both polar molecules and ions can induce the electrical signal reduction, and distinguish liquids with different molecules and ions can be achieved by analyzing output signals and resistance changes. The other reported design for detecting liquid ethanol and water is constituted of polyamide 6,6 (PA) film or PTFE film.[70b] The different surfaces exhibit distinctive affinity to water or ethanol, leading to different contact angles on the contact interface. As the PTFE surface is hydrophilic to the ethanol, dispersed droplets spread on the surface and construct an isolated layer. This layer impairs the electron depleting, and electron double-layer formation on the interface results in a sharp decline in the output performance. However, when water droplets drop onto the surface, an open-circuit voltage of up to 60 V is detected, and it continuously decreases with the addition of ethanol. The different affinity to water and ethanol enables a sensitive monitor for the ambient environment.

7. Perspectives and Conclusion

The mechanical energy harvester has been dominated by EMGs since the invention of the electromagnetic effect. However, the characteristics of EMGs require for high-quality energy source, which is relatively rare and hard to be utilized in nature. Due to the construction difficulties and low efficiency of EMGs with unstable triggers, TENGs are investigated for harvesting low-frequency energy in the ambient environment. The performance comparison of TENG with different modes is supplied in **Table 1**. In general, water TENGs have been demonstrated and implemented in numerous forms for harvesting hydropower, such as raindrops, river streams, ocean waves, etc. The harvested energy is considered as a promising candidate for renewable sources and remission of the energy crisis. However, TENGs are based on the CE phenomenon, which is demonstrated and explained with an electron cloud model for general forms. As mentioned in the former sections, the energy could induce a current and support the loaded equipment in the external circuit. Also, it can be directly used for self-powered sensors or actuators.

Table 1. Function modes of TENG and output performances.

Function mode	Output current	Output voltage	Power density	References
Contact separation	17.5 mA m^{-2}	300 V	2.0 W m^{-2}	[26]
Single electrode	238 nA	7 V	0.27 μW cm^{-2}	[62c]
Single electrode	–	–	≈170 μW	[24]
Single electrode	17 μA	9.3 V	145 μW	[22]
Sliding free-standing	5.3 μA	3.1 V	0.5 W m^{-2}	[28]
Sliding free-standing	>10 μA	15–20 mV s^{-1}	/	[31b]
Press releasing	–	8 V	0.3 μW cm^{-2}	[34]

Recently, the advancing of TENG has broken the limitation of the surface effect, varying from surface modifications to conceptual innovation.[65b,71] Xu et al. reported a PTFE-based TENG charge storage container based on impinging water.[71a] In this work, the PTFE film is not only applied as the water–solid interface but also transforms the interfacial effect of conventional TENGs to a bulk effect. After 1.6×10^4 times of collision, the surface charge reaches a saturation state of about 49.8 nC, and the open-circuit voltage is about 143.5 V. For self-powered wireless TENG, Zhang et al. build an analytic model relying on the magnetic resonance coupling capable of the efficiency of 73% for a 5 cm distance.[71b] The 3D fabrication[65b] and integrated structure[71e] for multiple-effects applications are also achieved. The sufficient improvement of TENG in both practical use and research is dedicated to two aspects. First, the design innovation of multifunctional energy models is vital. Even though the fundamental four modes have been established and widely implemented, the combinations of materials and structures should be unlimited. The fabrication and modification for improving energy harvesting efficiency are dominant in the development of TENGs. Second, systematical integration is also crucial for TENG innovation. Loose parts and complicated components would sometimes lead to immense problems, as the enclosed TENG for ocean wave energy harvesting. The development tendency has identified the importance of these problems, which would also suggest vast opportunities and prospects of TENGs. With these rapid promotions of the efficiency and applicable range of TENG devices, more endeavors are still highly desired to further investigate in this field to improve the performance of the TENG toward practical applications in blue energy harvesting.

Acknowledgements

The authors gratefully acknowledge the support of the Natural Science Foundation of China (Grant No.: NSFC 21771156), and the Early Career Scheme (ECS) fund (Grant No.: PolyU 253026/16P) from the Research Grant Council (RGC) in Hong Kong.

Conflict of Interest

The authors declare no conflict of interest.

Keywords

contact electrification, electron cloud models, electrostatic double layers, solid–liquid interface, triboelectric nanogenerators

Received: December 1, 2020
Revised: January 18, 2021
Published online: March 8, 2021

[1] Z. L. Wang, J. H. Song, *Science* **2006**, *312*, 242.
[2] F. R. Fan, Z. Q. Tian, Z. L. Wang, *Nano Energy*, **2012**, *1*, 328.
[3] F. R. Fan, W. Tang, Z. L. Wang, *Adv. Mater.* **2016**, *28*, 4283.
[4] Z. L. Wang, *Nanogenerators for Self-Powered Devices and Systems*, Georgia Institute of Technology, Atlanta, GA **2011**.
[5] G. Zhu, Y. S. Zhou, P. Bai, X. S. Meng, Q. Jing, J. Chen, Z. L. Wang, *Adv. Mater.* **2014**, *26*, 3788.
[6] W. Tang, T. Jiang, F. R. Fan, A. F. Yu, C. Zhang, X. Cao, Z. L. Wang, *Adv. Funct. Mater.* **2015**, *25*, 3718.
[7] F.-R. Fan, Z.-Q. Tian, Z. L. Wang, *Nano Energy* **2012**, *1*, 328.
[8] Y. Xie, S. Wang, S. Niu, L. Lin, Q. Jing, J. Yang, Z. Wu, Z. L. Wang, *Adv. Mater.* **2014**, *26*, 6599.
[9] C. Xu, Y. Zi, A. C. Wang, H. Zou, Y. Dai, X. He, P. Wang, Y. C. Wang, P. Feng, D. Li, Z. L. Wang, *Adv. Mater.* **2018**, *30*, e1706790.
[10] C. Xu, Y. Zi, A. C. Wang, H. Zou, Y. Dai, X. He, P. Wang, Y. C. Wang, P. Feng, D. Li, *Adv. Mater.* **2018**, *30*, 1706790.
[11] J. Nie, Z. Ren, L. Xu, S. Lin, F. Zhan, X. Chen, Z. L. Wang, *Adv. Mater.* **2020**, *32*, 1905696.
[12] C. Wu, A. C. Wang, W. Ding, H. Guo, Z. L. Wang, *Adv. Energy Mater.* **2019**, *9*, 1802906.
[13] Z. L. Wang, A. C. Wang, *Mater. Today* **2019**, *30*, 34.
[14] a) L. S. McCarty, G. M. Whitesides, *Angew. Chem. Int. Ed.* **2008**, *47*, 2188; b) Z. L. Wang, A. C. Wang, *Mater. Today* **2019**, *30*, 34.
[15] Z.-H. Lin, G. Cheng, W. Wu, K. C. Pradel, Z. L. Wang, *ACS Nano* **2014**, *8*, 6440.
[16] a) Y. S. Zhou, S. M. Li, S. M. Niu, Z. L. Wang, *Nano Res.* **2016**, *9*, 3705; b) Y. S. Zhou, Y. Liu, G. Zhu, Z. H. Lin, C. F. Pan, Q. S. Jing, Z. L. Wang, *Nano Lett.* **2013**, *13*, 2771.
[17] a) L.-H. Lee, *J Electrostat.* **1994**, *32*, 1-29; b) J. Lowell, A. Akande, *J. Phys. D: Appl. Phys.* **1988**, *21*, 125; c) F. Vick, *Br. J. Appl. Phys.* **1953**, *4*, S1.
[18] F. Liang, X. J. Zhao, H. Y. Li, Y. J. Fan, J. W. Cao, Z. L. Wang, G. Zhu, *Nano Energy* **2020**, *69*, 104414.
[19] P. Jiang, L. Zhang, H. Guo, C. Chen, C. Wu, S. Zhang, Z. L. Wang, *Adv. Mater.* **2019**, *31*, 1902793.
[20] Z. H. Lin, G. Cheng, L. Lin, S. Lee, Z. L. Wang, *Angew. Chem. Int. Ed.* **2013**, *52*, 12545.
[21] W. Tang, B. D. Chen, Z. L. Wang, *Adv. Funct. Mater.* **2019**, *29*, 1901069.
[22] Z. H. Lin, G. Cheng, S. Lee, K. C. Pradel, Z. L. Wang, *Adv. Mater.* **2014**, *26*, 4690.
[23] a) H. Zhang, Y. Yang, X. Zhong, Y. Su, Y. Zhou, C. Hu, Z. L. Wang, *ACS Nano* **2014**, *8*, 680; b) Y. Yang, H. Zhang, R. Liu, X. Wen, T. C. Hou, Z. L. Wang, *Adv. Energy Mater.* **2013**, *3*, 1563.
[24] Y. J. Sun, X. Huang, S. Soh, *Chem. Sci.* **2015**, *6*, 3347.
[25] J. Chung, D. Heo, B. Kim, S. Lee, *Micromachines* **2018**, *9*, 593.
[26] L. Wang, W. Liu, Z. Yan, F. Wang, X. Wang, *Adv. Funct. Mater.* **2020**, 2007221.
[27] W. He, M. Sohn, R. Ma, D. J. Kang, *Nano Energy* **2020**, *78*, 105383.
[28] S.-H. Kwon, J. Park, W. K. Kim, Y. Yang, E. Lee, C. J. Han, S. Y. Park, J. Lee, Y. S. Kim, *Energ. Environ. Sci.* **2014**, *7*, 3279.

[29] a) A. Ahmed, Z. Saadatnia, I. Hassan, Y. Zi, Y. Xi, X. He, J. Zu, Z. L. Wang, *Adv. Energy Mater.* **2017**, *7*, 1601705; b) Z.-H. Lin, G. Cheng, X. Li, P.-K. Yang, X. Wen, Z. L. Wang, *Nano Energy* **2015**, *15*, 256; c) S. Niu, Y. Liu, X. Chen, S. Wang, Y. S. Zhou, L. Lin, Y. Xie, Z. L. Wang, *Nano Energy* **2015**, *12*, 760; d) S. Wang, Y. Xie, S. Niu, L. Lin, Z. L. Wang, *Adv. Mater.* **2014**, *26*, 2818; e) D. Zhang, J. Shi, Y. Si, T. Li, *Nano Energy* **2019**, *61*, 132.

[30] a) H. Yong, J. Chung, D. Choi, D. Jung, M. Cho, S. Lee, *Sci. Rep.* **2016**, *6*, 33977; b) T. Kim, S. Jeon, S. Lone, S. J. Doh, D.-M. Shin, H. K. Kim, Y.-H. Hwang, S. W. Hong, *Nano Energy* **2018**, *54*, 209; c) H. Ryu, J. H. Lee, U. Khan, S. S. Kwak, R. Hinchet, S.-W. Kim, *Energ. Environ. Sci.* **2018**, *11*, 2057.

[31] a) Y. Su, X. Wen, G. Zhu, J. Yang, J. Chen, P. Bai, Z. Wu, Y. Jiang, Z. L. Wang, *Nano Energy* **2014**, *9*, 186; b) L. Helseth, X. Guo, *Smart Mater. Struct.* **2016**, *25*, 045007.

[32] a) G. Zhu, Y. Su, P. Bai, J. Chen, Q. Jing, W. Yang, Z. L. Wang, *ACS Nano* **2014**, *8*, 6031; b) X. J. Zhao, S. Y. Kuang, Z. L. Wang, G. Zhu, *ACS Nano* **2018**, *12*, 4280.

[33] a) X. Wang, S. Niu, Y. Yin, F. Yi, Z. You, Z. L. Wang, *Adv. Energy Mater.* **2015**, *5*, 1501467; b) L. Xu, T. Jiang, P. Lin, J. J. Shao, C. He, W. Zhong, X. Y. Chen, Z. L. Wang, *ACS Nano* **2018**, *12*, 1849.

[34] J. K. Moon, J. Jeong, D. Lee, H. K. Pak, *Nat. Commun.* **2013**, *4*, 1.

[35] S.-H. Shin, Y. H. Kwon, Y.-H. Kim, J.-Y. Jung, M. H. Lee, J. Nah, *ACS Nano* **2015**, *9*, 4621.

[36] a) X. Chen, L. Miao, H. Guo, H. Chen, Y. Song, Z. Su, H. Zhang, *Appl. Phys. Lett.* **2018**, *112*, 203902; b) Z. H. Lin, G. Zhu, Y. S. Zhou, Y. Yang, P. Bai, J. Chen, Z. L. Wang, *Angew. Chem. Int. Ed.* **2013**, *52*, 5065; c) A. I. Uddin, G.-S. Chung, *Sens. Actuators B Chem.* **2016**, *231*, 601; d) X.-S. Zhang, J. Brugger, B. Kim, *Nano Energy* **2016**, *20*, 37.

[37] J. Ding, W.-Q. Tao, S.-K. Fan, *Nano Energy* **2020**, *70*, 104473.

[38] a) H. Helmholtz, *Annalen der Physik und Chemie* **1853**, *165*, 211; b) M. Namisnyk, *J. AUPEC* **2003**, *1*, 51; c) A. A. Kornyshev, *J. Phys. Chem. B* **2007**, *111*, 5545; d) R. Zimmermann, S. Dukhin, C. Werner, *J. Phys. Chem. B* **2001**, *105*, 8544.

[39] a) M. Gouy, *J. Phys.* **1910**, *9*, 457; b) D. L. Chapman, *Philos. Mag.* **1913**, *25*, 475; c) K. B. Oldham, *J. Electroanal. Chem.* **2008**, *613*, 131.

[40] C. W. Outhwaite, L. B. Bhuiyan, S. Levine, *J. Chem. Soc., Faraday Trans.* 2 **1980**, *76*, 1388.

[41] G. Quincke, *Ann. Phys.* **1859**, *183*, 1.

[42] F. H. van der Heyden, D. Stein, C. Dekker, *Phys. Rev. Lett.* **2005**, *95*, 116104.

[43] R. Zhang, S. Wang, M. H. Yeh, C. Pan, L. Lin, R. Yu, Y. Zhang, L. Zheng, Z. Jiao, Z. L. Wang, *Adv. Mater.* **2015**, *27*, 6482.

[44] a) A. Yaroshchuk, T. Luxbacher, *Langmuir* **2010**, *26*, 10882; b) R. Schweiss, P. B. Welzel, C. Werner, W. Knoll, *Colloids Surf. A Physicochem. Eng. Asp.* **2001**, *195*, 97; c) J. F. Duval, R. Zimmermann, A. L. Cordeiro, N. Rein, C. Werner, *Langmuir* **2009**, *25*, 10691.

[45] a) A. E. Cohen, *Science* **2003**, *300*, 1235; b) P. Dhiman, F. Yavari, X. Mi, H. Gullapalli, Y. Shi, P. M. Ajayan, N. Koratkar, *Nano Lett.* **2011**, *11*, 3123.

[46] R. Liu, C. Liu, S. Fan, *ACS Appl. Mater. Interfaces* **2018**, *10*, 35273.

[47] a) J. Yin, X. Li, J. Yu, Z. Zhang, J. Zhou, W. Guo, *Nat. Nanotech.* **2014**, *9*, 378; b) J. Yin, Z. Zhang, X. Li, J. Yu, J. Zhou, Y. Chen, W. Guo, *Nat. Commun.* **2014**, *5*, 1.

[48] X. Wang, Z. Wen, H. Guo, C. Wu, X. He, L. Lin, X. Cao, Z. L. Wang, *ACS Nano* **2016**, *10*, 11369.

[49] A. Cassie, S. Baxter, *Trans. Faraday Soc.* **1944**, *40*, 546.

[50] H. J. Ensikat, A. J. Schulte, K. Koch, W. Barthlott, *Langmuir* **2009**, *25*, 13077.

[51] a) I. S. Bayer, F. Brandi, R. Cingolani, A. Athanassiou, *Colloid. Polym. Sci.* **2013**, *291*, 367; b) J.-W. Lee, W. Hwang, *Nano Energy* **2018**, *52*, 315.

[52] X. Pu, W. Song, M. Liu, C. Sun, C. Du, C. Jiang, X. Huang, D. Zou, W. Hu, Z. L. Wang, *Adv. Energy Mater.* **2016**, *6*, 1601048.

[53] L. Pan, J. Wang, P. Wang, R. Gao, Y.-C. Wang, X. Zhang, J.-J. Zou, Z. L. Wang, *Nano Res.* **2018**, *11*, 4062.

[54] J. Wang, Z. Wu, L. Pan, R. Gao, B. Zhang, L. Yang, H. Guo, R. Liao, Z. L. Wang, *ACS Nano* **2019**, *13*, 2587.

[55] B. D. Chen, W. Tang, C. He, T. Jiang, L. Xu, L. P. Zhu, G. Q. Gu, J. Chen, J. J. Shao, J. J. Luo, *Adv. Mater. Technol.* **2018**, *3*, 1700229.

[56] Y. Wu, Y. Su, J. Bai, G. Zhu, X. Zhang, Z. Li, Y. Xiang, J. Shi, *J. Nanomater.* **2016**, *2016*, 5121572.

[57] a) J. Wang, C. Wu, Y. Dai, Z. Zhao, A. Wang, T. Zhang, Z. L. Wang, *Nat. Commun.* **2017**, *8*, 1; b) Y. Zi, J. Wang, S. Wang, S. Li, Z. Wen, H. Guo, Z. L. Wang, *Nat. Commun.* **2016**, *7*, 1; c) J. Chen, J. Yang, Z. Li, X. Fan, Y. Zi, Q. Jing, H. Guo, Z. Wen, K. C. Pradel, S. Niu, *ACS Nano* **2015**, *9*, 3324; d) T. Jiang, L. M. Zhang, X. Chen, C. B. Han, W. Tang, C. Zhang, L. Xu, Z. L. Wang, *ACS Nano* **2015**, *9*, 12562.

[58] T. Jiang, Y. Yao, L. Xu, L. Zhang, T. Xiao, Z. L. Wang, *Nano Energy* **2017**, *31*, 560.

[59] a) G. Cheng, Z.-H. Lin, Z.-L. Du, Z. L. Wang, *ACS Nano* **2014**, *8*, 1932; b) D. Jiang, F. Guo, M. Xu, J. Cai, S. Cong, M. Jia, G. Chen, Y. Song, *Nano Energy* **2019**, *58*, 842; c) T. Kim, J. Chung, D. Y. Kim, J. H. Moon, S. Lee, M. Cho, S. H. Lee, S. Lee, *Nano Energy* **2016**, *27*, 340; d) Q. Liang, X. Yan, Y. Gu, K. Zhang, M. Liang, S. Lu, X. Zheng, Y. Zhang, *Sci. Rep.* **2015**, *5*, 1.

[60] a) D. Yoo, S.-C. Park, S. Lee, J.-Y. Sim, I. Song, D. Choi, H. Lim, D. S. Kim, *Nano Energy* **2019**, *57*, 424; b) Y. Liu, N. Sun, J. Liu, Z. Wen, X. Sun, S.-T. Lee, B. Sun, *ACS Nano* **2018**, *12*, 2893; c) Y. C. Lai, Y. C. Hsiao, H. M. Wu, Z. L. Wang, *Adv. Sci.* **2019**, *6*, 1801883; d) L. Zheng, Z.-H. Lin, G. Cheng, W. Wu, X. Wen, S. Lee, Z. L. Wang, *Nano Energy* **2014**, *9*, 291; e) Q. Zhou, J. G. Park, K. N. Kim, A. K. Thokchom, J. Bae, J. M. Baik, T. Kim, *Nano Energy* **2018**, *48*, 471.

[61] a) S.-H. Kwon, W. K. Kim, J. Park, Y. Yang, B. Yoo, C. J. Han, Y. S. Kim, *ACS Appl. Mater. Interfaces* **2016**, *8*, 24579; b) J. Tian, X. Chen, Z. L. Wang, *Nanotechnology* **2020**, *31*, 242001; c) S.-B. Jeon, D. Kim, G.-W. Yoon, J.-B. Yoon, Y.-K. Choi, *Nano Energy* **2015**, *12*, 636; d) Y. Cho, S. Lee, J. Hong, S. Pak, B. Hou, Y.-W. Lee, J. E. Jang, H. Im, J. I. Sohn, S. Cha, *J. Mater. Chem. A* **2018**, *6*, 12440.

[62] S. Wang, L. Lin, Z. L. Wang, *Nano Energy* **2015**, *11*, 436.

[63] Z. L. Wang, *ACS Nano* **2013**, *7*, 9533.

[64] a) T. Yang, D. Xie, Z. Li, H. Zhu, *Mater. Sci. Eng.: Rep.* **2017**, *115*, 1; b) C. Chen, L. Chen, Z. Wu, H. Guo, W. Yu, Z. Du, Z. L. Wang, *Mater. Today* **2020**, *32*, 84.

[65] G. Zhu, W. Q. Yang, T. Zhang, Q. Jing, J. Chen, Y. S. Zhou, P. Bai, Z. L. Wang, *Nano Lett.* **2014**, *14*, 3208.

[66] S. Park, J. Park, Y.-G. Kim, S. Bae, T.-W. Kim, K.-I. Park, B. H. Hong, C. K. Jeong, S.-K. Lee, *Nano Energy* **2020**, *78*, 105266.

[67] a) Q. Shi, T. He, C. Lee, *Nano Energy* **2019**, *57*, 851; b) Z. L. Wang, *ACS Nano* **2013**, *7*, 9533; c) W. Seung, M. K. Gupta, K. Y. Lee, K.-S. Shin, J.-H. Lee, T. Y. Kim, S. Kim, J. Lin, J. H. Kim, S.-W. Kim, *ACS Nano* **2015**, *9*, 3501.

[68] a) S. Wang, G. Xie, H. Tai, Y. Su, B. Yang, Q. Zhang, X. Du, Y. Jiang, *Nano Energy* **2018**, *51*, 231; b) S. Cui, Y. Zheng, T. Zhang, D. Wang, F. Zhou, W. Liu, *Nano Energy* **2018**, *49*, 31; c) S. Gao, Y. Zhu, Y. Chen, M. Tian, Y. Yang, T. Jiang, Z. L. Wang, *Mater. Today* **2019**, *28*, 17.

[69] a) X. Li, M.-H. Yeh, Z.-H. Lin, H. Guo, P.-K. Yang, J. Wang, S. Wang, R. Yu, T. Zhang, Z. L. Wang, *ACS Nano* **2015**, *9*, 11056; b) H. Zhang, Y. Yang, Y. Su, J. Chen, C. Hu, Z. Wu, Y. Liu, C. P. Wong, Y. Bando, Z. L. Wang, *Nano Energy* **2013**, *2*, 693.

[70] W. Kim, D. Choi, J.-Y. Kwon, D. Choi, *J. Mater. Chem. A* **2018**, *6*, 14069.
[71] a) W. Xu, H. Zheng, Y. Liu, X. Zhou, C. Zhang, Y. Song, X. Deng, M. Leung, Z. Yang, R. X. Xu, *Nature* **2020**, *578*, 392; b) C. Zhang, J. Chen, W. Xuan, S. Huang, B. You, W. Li, L. Sun, H. Jin, X. Wang, S. Dong, *Nat. Commun.* **2020**, *11*, 1; c) J. Wang, Y. Li, Z. Xie, Y. Xu, J. Zhou, T. Cheng, H. Zhao, Z. L. Wang, *Adv. Energy Mater.* **2020**, 1904227; d) W. Wang, A. Yu, X. Liu, Y. Liu, Y. Zhang, Y. Zhu, Y. Lei, M. Jia, J. Zhai, Z. L. Wang, *Nano Energy* **2020**, *71*, 104605; e) K. Zhao, B. Ouyang, C. R. Bowen, Z. L. Wang, Y. Yang, *Nano Energy* **2020**, *71*, 104632.

Bolong Huang received his B.Sc. degree from Peking University in 2007 and his Ph.D. degree from the University of Cambridge in 2012. Following a systematic training period as a research assistant at Peking University and Hong Kong, he is currently an assistant professor at the Hong Kong Polytechnic University. His main research fields are theoretical calculations of electronic structures on nanomaterials, energy materials, solid functional materials, and rare-earth materials, as well as their applications in multi-scale energy conversion and supply systems.

Zhong Lin Wang is the hightower chair in materials science and engineering, regents' professor, and engineering distinguished professor at Georgia Tech. He is also the chief scientist and director of the Beijing Institute of Nanoenergy and Nanosystems, Chinese Academy of Sciences. His discovery and breakthroughs in nanogenerators establish the principle and technological road map for harvesting mechanical energy from environment and biological systems for powering personal electronics. His research on self-powered nanosystems has inspired worldwide efforts in academia and industry for studying energy for micro-nanosystems, which is now a distinct disciplinary in energy research and future sensor networks.